Clim. Past Discuss., https://doi.org/10.5194/cp-2018-157
Manuscript under review for journal Clim. Past
Discussion started: 7 December 2018

Climate of the Past Discussions
Open Access
EGU

Late Miocene to Recent High Resolution Eastern Equatorial Pacific Carbonate Records: Stratigraphy linked by dissolution and paleoproductivity

Mitchell Lyle[1], Anna Joy Drury[2], Jun Tian[3], Roy Wilkens[4], and Thomas Westerhold[2]

[1]College of Earth, Ocean, and Atmospheric Science, Oregon State University, 104 CEOAS Admin Bldg, Corvallis, Oregon 97331, USA
[2]MARUM-Center for Marine Environmental Sciences, University of Bremen, Leobener Strasse, DE-28359 Bremen, Germany
[3] Laboratory of Marine Geology, Tongji University, Siping Road 1239, Shanghai 200092, PR China
[4] University of Hawaii, School of Ocean and Earth Science and Technology, Honolulu Hawaii 96822, USA

Correspondence to: Mitchell Lyle (mlyle@coas.oregonstate.edu)

Abstract. We report late Miocene-Recent time series of XRF-derived bulk sediment composition and *mass accumulation rates* (MAR) from IODP Sites U1335, U1337, U1338 and ODP Site 849, and also report bulk density-derived $CaCO_3$ MAR at Sites 848, 850 and 851. We use physical properties and images to intercorrelate all records for the last 8 Myr with resolutions of 1-2 kyr. Large magnitude changes in $CaCO_3$ and opal MAR occurred within that time period but clay deposition has remained relatively constant. Ratios of $CaCO_3$ % or SiO_2% to clay can be used to emulate biogenic MAR. We define 5 major *Plio-Pleistocene Low $CaCO_3$ %* (PPLC) intervals since 5.3 Ma. Two were caused primarily by high opal burial that diluted $CaCO_3$ (PPLC-2—1685-2135 ka, and PPLC-5—4465-4737 ka), while 3 were caused by enhanced dissolution of $CaCO_3$ (PPLC-1—51-402 ka, PPLC-3—2248-2684 ka, and PPLC-4—2915-4093 ka). Regional patterns of $CaCO_3$ % minima can distinguish between lows caused by high diatom production versus lows caused by dissolution. High diatom production causes lowest $CaCO_3$% at equatorial locations, while higher dissolution causes lowest $CaCO_3$ at higher latitudes. The dissolution interval PPLC-4 occurs as the Central American Seaway closed and during a long decline from extreme positive Atlantic-Pacific carbon isotope gradients indicating an abyssal Pacific buildup of uncompensated DIC in the early Pliocene. The two major post-Miocene production intervals, PPLC-2 and PPLC-5, have different geographic footprints because of regional changes in eastern Pacific nutrient storage after the closure of the Panama Seaway.

1 Introduction

The Cenozoic sediments of the eastern tropical Pacific Ocean have recorded changes in productivity and the Pacific deep carbon reservoir (Berger, 1973; van Andel et al, 1975; Pälike et al, 2012). Distinctive $CaCO_3$ profiles can be correlated across thousands of km within the eastern equatorial Pacific because of coherent variability within the region (Mayer et al, 1986). Modern coherent climate variability is exhibited across the eastern tropical Pacific by the large-scale response to

Clim. Past Discuss., https://doi.org/10.5194/cp-2018-157
Manuscript under review for journal Clim. Past
Discussion started: 7 December 2018

ENSO (Mantua et al, 1997; Di Lorenzo et al, 2015). Since $CaCO_3$ variability causes the sediment bulk density to vary (Mayer, 1991), the extensive geographic scale of these major $CaCO_3$ changes produces a distinctive set of seismic reflection horizons (Bloomer and Mayer, 1997; Tominaga et al., 2011) linked with major paleoceanographic change in the Pacific Ocean (Mayer et al, 1986).

The change in the calcite compensation depth (CCD) in the world's oceans is a primary indicator of rearrangement of the global carbon cycle. Well-known major changes in CCD are associated with the major climate changes of the Cenozoic (Berger, 1973; van Andel and Moore, 1974; Peterson et al., 1992; Pälike et al., 2012). Fluctuations in the CCD represent changes in the balance between $CaCO_3$ production in surface waters and $CaCO_3$ dissolution of carbonate hard parts at the benthic boundary layer (Milliman and Droxler, 1996; Boudreau et al., 2010). Once buried, pore water concentrations quickly reach saturation with respect to $CaCO_3$ and the remaining $CaCO_3$ is preserved. The CCD shallows when either (a) lower carbonate production results in lower carbonate rain to the seafloor, (b) the $[CO_3]^{2-}$ content of bottom water decreases and becomes undersaturated with respect to calcite, or (c) rising sea levels allow significantly more $CaCO_3$ storage on continental shelves and shallow basins (Opdyke and Wilkinson, 1988). .

Higher CO_2 outgassing from the mantle or released by degradation of terrestrial soils and/or biosphere results in net CO_2 transfer to the atmosphere and oceans. Global changes in CCD can therefore reflect the rate of change of CO_2 outgassing versus the rate at which weathering consumes atmospheric CO_2 and adds cations to the oceans (Zeebe and Caldeira, 2008). A fast CO_2-weathering response is a strong negative feedback and should minimize the depth change of the CCD and the pace and duration of these changes. Tracking carbonate dissolution thus gives important information not only about when perturbations in the carbon cycle have occurred but also about the speed and strength of the weathering response to a CO_2 transient.

The CCD differs between ocean basins (Berger, 1970) because ocean circulation shifts the deep ocean location where uncompensated DIC produced by water column degradation of organic matter resides and where $CaCO_3$-unsaturated water impinges on sediments. The Holocene deep Atlantic Ocean is flushed with high alkalinity, low DIC water originating from the surface North Atlantic that causes a much deeper CCD than that in the Pacific. The Atlantic CCD shallows in glacials because of the loss of NADW, while the Pacific CCD deepens as more low $[CO_3]^{2-}$ water intrudes into the Atlantic basin and dissolves $CaCO_3$ there.

The CCD has varied both on glacial-interglacial scales and over long periods of time. Since large areas of the abyssal ocean basins are subject to $CaCO_3$ dissolution, variation imposes a common regional $CaCO_3$ stratigraphy modulated by the CCD change. Such a common chronostratigraphic signal in the eastern equatorial Pacific has been noted through the Cenozoic [Hays et al, 1969; Mayer et al, 1986; Chuey et al, 1987; Farrell and Prell, 1989; Farrell and Prell, 1991].

Clim. Past Discuss., https://doi.org/10.5194/cp-2018-157
Manuscript under review for journal Clim. Past
Discussion started: 7 December 2018

The development of the typical eastern Pacific $CaCO_3$ burial profile is complicated by large-scale long-term variation in biogenic production (Farrell et al, 1995; Lyle and Baldauf, 2015). Such variability can change the dissolution-related $CaCO_3$ signal by changing the relative proportion of $CaCO_3$ to biogenic opal in the rain of biogenic hard parts. Nevertheless, knowledge of the processes that modify $CaCO_3$ deposition allows for common intervals to be identified. The major low $CaCO_3$ intervals we report are longer than that of the typical precession/obliquity-related Milankovitch orbital forcing, ranging from 150 to 460 kyr in length.

In this paper, we present 8 Myr long orbitally-resolving records of bulk sediment composition. We will briefly discuss the late Miocene to Holocene evolution of biogenic sedimentation in the equatorial Pacific. We will then update the long-period carbonate stratigraphy for the period between 0 and 5.3 Ma and will show the similarities and differences between the carbonate records from different drill sites. We choose 5.3-0 Ma because it has good age control and contains examples of most of the major Neogene factors that change $CaCO_3$ profiles in the equatorial Pacific. It includes the last major diatom deposition interval within the Late Miocene Biogenic Bloom (LMBB) in addition to low $CaCO_3$ intervals related to excess dissolution in the Pliocene. The period between 4.5 and 8 Ma, the LMBB, is an interval dominated by high surface production and deposition at the equator west of 100°W. There is clear geographic variability in the LMBB that requires further work in order to sort out the detailed changes with longitude, define stratigraphic tie points with additional sites, and to understand processes that led to the regional productivity response.

We use a combined age model made by joining a Site 849 stable isotope record (data from Mix et al, 1995) correlated to the new Ceara Rise stack age model (Wilkens et al., 2017) for the 0-3.5 Ma interval. This was joined to the astronomically tuned age model for the Site U1338 stable isotope record that spans from 3.5-8.2 Ma (Drury et al, 2016, 2018).

Sediment composition data combined with the age model were used to calculate mass accumulation rates (MAR) to study regional deposition patterns in the eastern tropical Pacific. We also use ratios of opal to clay as an alternative method to determine periods of high diatom production of bio-silica. We found that the ratio of XRF-determined $CaCO_3$ to $BaSO_4$ is a useful measure of relative dissolution, since Ba rain is more consistently preserved and is well correlated with export C_{org} rain (Dymond and Collier, 1996) and $CaCO_3$ rain is proportional to export C_{org} production (Honjo et al, 1995; Lyle and Baldauf, 2015).

2 Drill Sites Studied

We report data from 7 equatorial Pacific drillsites, 4 with XRF scans along the sediment splice (IODP Sites U1335, U1337, U1338, ODP Site 849) and 4 with $CaCO_3$ data estimated from spliced GRA wet bulk density profiles (ODP Sites 848, 849,

850 and 851; see Methods for the process). Locations for the drill sites are shown in Figure 1 and in Table 1. The drill sites from ODP Leg 138 range from 3°S to 2.8°N along the ODP Leg 138 110°W transect (Mayer et al., 1992) and Neogene sites from IODP Exp 320/321 drilled as part of the Cenozoic Equatorial Megasplice (Pälike et al, 2010a). The Leg 138 sites have been cored to basement, aged about 11 Ma along 110°W. The Exp 320/321 sites were also cored to basement but are on progressively older basement displaced further north along a common flow line from the east Pacific Rise. Because they are on older ocean crust, the Exp 320/321 sites have sediment records that extend back into the early Miocene and late Oligocene (Pälike et al, 2010a).

All 7 sites have continuous orbital-resolving records of estimated $CaCO_3$, with ages for the 0-8.2 Ma section from this study. $CaCO_3$ was estimated from GRA bulk density for the entire sediment section (~11 Ma) for the ODP Leg 138 Sites 848, 849, 850, and 851. Site U1335 has XRF measurements and XRF $CaCO_3$ to 300 m ccsf (~21 Ma), while Site U1337 and Site U1338 have XRF and XRF estimated $CaCO_3$ to basement (~24 Ma and ~17 Ma, respectively; Lyle et al, 2012, Wilson, 2014). Site 849 was XRF scanned to 287 m ccsf (7.2 Ma) so has $CaCO_3$ estimated by both GRA bulk density and XRF. When compared with shipboard measurements of $CaCO_3$ % at Site 849, the XRF estimate (sd of difference from measured: ±3.86%) is somewhat better than the GRA $CaCO_3$ % estimate (sd of difference from measured ±5.86%; see Figure SM-4 in the supplemental material) although both find the same trends.

Because Drury et al (2016, 2018) created an astronomically tuned stable isotope stratigraphy from 3.5 to 8.2 Ma that we could splice and depth match to the Site 849 stable isotope data spanning 0 to 5.0 Ma, we have extended age and sediment composition data to either 8.2 Ma or the base of the XRF data at all sites (Supplemental tables SM-17 through SM-21).

The seven sites span the equatorial Pacific productivity zone and extend from 3°S to 5.3°N (Table 1). At 5 Ma, the sites span from ~4°S to ~4°N. All of the sites are west of the East Pacific Rise and contain sediments that are primarily biogenic in origin. Sites that are further from the equator and/or deeper have more clay in the sediments (U1335, U1337, 851) than those shallower and nearer the equator, partly because of lower carbonate production and preservation but also because of higher dust deposition near the ITCZ, located north of the equator (Hovan, 1995).

Primarily because of depth dependent carbonate dissolution, Site U1338 has a sedimentation rate only 75% of that at Site 851, which lies at the same latitude but on ocean crust that is half the age of Site U1338 and 450 m shallower. From 5.3 Ma to the Holocene each site deepened by about 200 m because of crustal cooling partly mitigated by sediment deposition shallowing the sea floor. Isostatic subsidence due to sediment loading increased the depth somewhat but subsidence is only ~20% of the added sediment thickness (Lyle, 1997). While significant changes in depth have happened to the 7 drill sites because of crustal cooling and sedimentation, the sites always remained separated by a similar water depth.

Clim. Past Discuss., https://doi.org/10.5194/cp-2018-157
Manuscript under review for journal Clim. Past
Discussion started: 7 December 2018

3 Methods

Please see the supplemental material for more information about the assembly and calibration of these data, including the age model, stratigraphic tie points, revised splices, estimated $CaCO_3$% profiles, and XRF bulk chemical data.

3.1 Stratigrapic Correlation of eastern Pacific drill sites

We used the Code for Ocean Drilling Data (CODD; https://www.codd-home.net/) analytical suite of software tools described by Wilkens et al (2017) for the stratigraphic correlation of all the drillsites. Initial correlations were made with the shipboard physical properties data from ODP or IODP collected by Multi-Sensor Track systems (MST), primarily magnetic susceptibility and GRA bulk density for this set of cores. If XRF and stable isotope data were available, the correlations were refined with this additional information.

The spliced sediment section at each drill site was stretched/squeezed to match the splice of a base or master drill site so that the sediment section could be expressed in the equivalent depth of the base site. Sites U1335, U1337, 851, and 849 were tied to U1338 as the base site, while sites 848 and 850 were tied to Site 849. The CODD analytical suite allows age datum levels like magnetochrons and biostratigraphic boundaries to be displayed in the correlation space, and these were used to constrain the depth matching. Depth ties between drill sites can be found in Supplemental Tables SM-8 to SM-13

3.2 The combined Site 849-Site U1338 age model

A combined age model was generated for all the sites by developing an age model for Site 849 from Mix et al (1995) benthic isotope data, and combining it with new astrochronology covering 3.5 Ma to 8.2 Ma at Site U1338 from Drury et al (2016, 2018). The age model was propagated to the other sites through use of the site-to-site correlations derived from the depth matched physical properties and bulk composition profiles. The isotope splice for Site 849 was assigned ages by correlation to the new Ceara Rise composite isotope stack in Wilkens et al (2017) to provide age control between 0-5.3 Ma. For U1338, we used the astrochronology developed by Drury et al. (2018) for Site U1338 between 3.5-8.0 Ma, which revised the benthic stable isotope age model in Drury et al (2016): based on depth matching between U1337 and U1338, the better astro-magnetochronology from Site U1337 constrained ages at Site U1338 through the late Miocene (8.0-6.0 Ma), while the remaining 6.0-3.5 Ma interval was astronomically tuned using the benthic $\delta^{18}O$ data (Drury et al, 2017; Drury et al., 2018). The 849 and U1338 age models were grafted together at 3626 ka to make the combined Site 849-U1338 age model, with Site 849 providing the younger section and Site U1338 providing the older one. See the supplemental material for more details and for the age model.

Clim. Past Discuss., https://doi.org/10.5194/cp-2018-157
Manuscript under review for journal Clim. Past
Discussion started: 7 December 2018

3.3 XRF scanning at Sites U1335, U1337, and U1338

The major elements (Al, Si, K, Ca, Fe) and significant minor elements (Ti, Mn, Ba) were measured with scanning XRF for Sites 849, U1335, U1337, and U1338 (Lyle et al, 2012; Shackford et al., 2014; Wilson, 2014). The element data was processed using the normalized, median-scaled (NMS) method of Lyle et al (2012), and then the data for U1337 and U1338 were calibrated with ICP-MS analyses of bulk sediment (Lyle et al, 2012; Wilson, 2014). NMS data were calibrated to shipboard $CaCO_3$ measurements to estimate $CaCO_3$ in all of the XRF sites (Lyle and Backman, 2013). In addition, opal was measured on discrete samples from 3 sites (849, U1338, U1337) to calibrate an XRF opal estimate. Clay was estimated by assuming that clay has constant TiO_2 and using the calibrated XRF TiO_2 estimate. Clay is assumed to have the same composition as Taylor and McLennan (1995) upper continental crust, which has 0.3% Ti. Clay-bound Si was estimated using the Taylor and McLennan (1995) Si/Ti ratio for upper continental crust. Opal was calibrated to the total Si minus the clay component (Lyle and Baldauf, 2015). See the supplemental material for more details.

3.4 $CaCO_3$ % estimates from GRA wet bulk density, Sites 848, 849, 850, and 851

It has long been known that variations in bulk density in the eastern equatorial Pacific are correlated to changes in $CaCO_3$ content (Mayer, 1991; Hagelberg et al., 1995). After removing the increasing bulk density trend caused by burial compaction, the variation in the decompacted bulk density can be used to quantitatively estimate $CaCO_3$. Unfortunately, Hagelberg et al (1995) did not publish their $CaCO_3$ estimates for the Leg 138 Sites, so we redid the estimate for Sites 848, 850, and 851 along the revised splices presented here. More detail about the estimate and data tables are in the supplemental material. We also estimated $CaCO_3$ at Site 849 from bulk density in addition to the XRF estimate in order to compare the two estimates.

3.5 Mass Accumulation Rate (MAR) calculation

The percentage data at each site were converted to MAR using the Site 849-U1338 age model, measured physical properties, and the bulk chemical data. The composition and physical properties data were interpolated to even 1-2 kyr spacing, then smoothed with a 20-point binomial filter before being resampled at 10-kyr intervals to accommodate probable errors in the age model and site-to-site correlations. MAR calculations are much more sensitive to age errors than age profiles of sediment components because they depend on the differential of depth vs time (sedimentation rate) as well as the time-depth correlation at each site. Bulk MAR was calculated by multiplying the dry bulk density by the sedimentation rate from the age-depth relationship. Individual component MARs were calculated by multiplying by the fraction of that component in the dry sample by the bulk MAR.

Opal (bio-SiO_2) $BaSO_4$, and clay MAR records were created at the sites where both XRF data and independent discrete measurements for opal and a clay-bound element existed. The XRF scanning data for Sites U1337 and U1338 were calibrated by ICP-MS analysis of the bulk sediment (Wilson, 2014; Lyle and Baldauf, 2015) along with separate opal

Clim. Past Discuss., https://doi.org/10.5194/cp-2018-157
Manuscript under review for journal Clim. Past
Discussion started: 7 December 2018

analysis of sediment samples using dissolution with KOH (Olivarez Lyle and Lyle, 2002). We used TiO_2 to estimate the clay amount and clay-bound SiO_2 for Sites U1337 and U1338. Unfortunately, discrete chemical analyses were never done for Site U1335, so that only the $CaCO_3$ record is calibrated at this time. Ratios of Si to Ti from Site U1335 suggest that the sediments have low opal contents. For Site 849, we correlated the XRF Fe_2O_3 NMS to a ^{232}Th estimate of clay from the upper part of the sediment column (Winckler et al, 2008). We used the XRF Fe_2O_3 because Ti contents were often below the XRF detection limit deeper than 130 m CCSF and because the oxide bound Fe is minimal. We used barite data from Ma et al. (2015) to calibrate the Site 849 XRF Ba data, and used our unpublished opal analyses using the KOH dissolution technique (Olivarez Lyle and Lyle, 2002) to calibrate the Site 849 XRF opal.

4 Eastern Tropical Pacific Sedimentation since 10 Ma

Biogenic sedimentation in the eastern tropical Pacific has not been constant over the last 10 million years. There was a major low $CaCO_3$ transient between 10 and 8 Ma known as the late Miocene carbonate crash (Lyle et al, 1995, Farrell et al, 1995; Roth et al, 2000). Between 8 and about 4.5 Ma, the equatorial region west of the East Pacific Rise experienced what is referred to as the late Miocene Biogenic Bloom (LMBB; Farrell et al, 1995; Lyle and Baldauf, 2015), a period with consistently high sedimentation rates and biogenic deposition but where opal and $CaCO_3$ burial varied considerably.

The difference in sedimentation is easily observed by the change in slope of the age-depth curves at about 4400 ka (Fig 2). Each drill site exhibits slower sedimentation rates after ~4400 ka, marking the end of the LMBB. In Figure 1, the spatial pattern of the LMBB is also shown by a ratio of the thickness of the older sediments (8-4.5 Ma) to that of the younger ones (4.5-0 Ma). Because there are only two time markers, other sites from Leg 138 can be included in the map (Sites 844, 845, 846, 847, 852, 853, and 854) as well as sites from ODP Leg 202 (Sites 1238, 1239, and 1241) and DSDP Sites (83, 158, and 572). Despite the shorter total time span and added compaction for the older section, the amount of sediment section deposited during the 8-4.5 Ma time interval is typically more than that deposited later in drill sites just north of the equator. The largest ratios mark the fastest deposition during the LMBB and are found in the region from roughly 88°W to 120°W, just north of the modern equator (orange shading in Figure 1). Factoring in Pacific plate motion, these sites were at the equator around 6-7 Ma. Drill sites from eastern corner of the equatorial Pacific do not have high deposition during the LMBB, although the interval in the east is marked by multiple intervals of high opal deposition as well (Farrell et al., 1995). The difference in sedimentation has been attributed to nutrient trapping in the easternmost Pacific and increased biogenic sediment production after the Central American Seaway closed (Farrell et al, 1995).

Profound changes in equatorial Pacific biogenic deposition from the middle Miocene to Recent were recorded at Site U1338 (Lyle and Baldauf, 2015). Dilution of $CaCO_3$ by opal deposition appears to be relatively common in the middle and late Miocene (Holbourn et al, 2014; Lyle and Baldauf, 2015). Fundamentally, a production-related low $CaCO_3$ interval can be

Clim. Past Discuss., https://doi.org/10.5194/cp-2018-157
Manuscript under review for journal Clim. Past
Discussion started: 7 December 2018

caused by much higher relative deposition of opal; $CaCO_3$ MAR may actually be higher within that interval but the increased $CaCO_3$ MAR is significantly less than the opal MAR increase, resulting in lower $CaCO_3$ %. For the most part, $CaCO_3$ burial was high through the Miocene, except within the late Miocene carbonate crash, 11-8 Ma. Poorest $CaCO_3$ preservation occurred at about 9.7 Ma (Lyle et al., 1995; Lyle and Baldauf, 2015). $CaCO_3$ preservation at Site U1338 was derived not only using the ratio of $CaCO_3$ to bio-$BaSO_4$, but is also by benthic/planktic foraminifera ratios (Pälike et al, 2010b). High opal % in sediments mostly reflects high opal deposition, but is superimposed over elevated dissolution of $CaCO_3$ during the late Miocene Carbonate Crash interval. Not only are ratios and MAR variable throughout the late Miocene, but the types of diatoms and their rates of burial varied as well. In the LMBB, the most diatom-rich intervals are a mixture of mat forming and upwelling diatom species, but the upwelling species extended over much longer time ranges than the high diatom deposition intervals and are not restricted to them. Northern subtropical diatoms were abundant at the beginning of the LMBB, and were replaced by diatoms now associated with the southern hemisphere subtropics (Lyle and Baldauf, 2015).

Clearly there has been a major evolution of equatorial productivity regime between 8 and 4.5 Ma. While the new age model for Site U1338 used in this paper is much better resolved than that used in Lyle and Baldauf (2015), similar patterns are apparent with the finer age resolution of the new age model (Fig 3). Changes in biogenic deposition apparently result from variable responses under different nutrient/upwelling conditions by different organisms. The observed responses apparently exceed the envelope encompassed by seasonal change in the JGOFS Pacific sediment trap experiment (Honjo et al, 1995; Dymond and Collier, 1996). Further work to understand the biogeochemical response should be done. Not only were there long intervals of high biogenic deposition, but also the ratios of the different biogenic hard parts varied by large amounts and different species within the phytoplankton participated at different times.

We have limited this paper to describe the factors that have shaped $CaCO_3$ % and MAR profiles since 5.3 Ma, the Pliocene and Pleistocene, because of the good age control within the interval and because there are good examples of both production and dissolution dominated intervals. We have found that the structure caused by changes in $CaCO_3$ production has a latitudinal component, while dissolution signals are more widespread but are strongest at deep sites underneath lower productivity in a roughly longitudinal pattern. Furthermore, a 100-kyr cyclicity of $CaCO_3$ content appears at about between 1.5 and 2 Ma and increases to the present, much earlier than the 100-kyr cycles of oxygen isotopes.

5 Results

The $CaCO_3$ % and $CaCO_3$ MAR profiles at all seven sites exhibit long period variability and orbital cyclicity (Figures 4 and 5). We have used the $CaCO_3$ % profiles to define five low long-period $CaCO_3$ % transients (Pliocene-Pleistocene Low $CaCO_3$ intervals, PPLCs) in Table 2. We use $CaCO_3$ % rather than MAR because (1) the percentage profiles can be directly measured as the sediment sections are processed, (2) the $CaCO_3$ % variability is chronostratigraphic across the east central

Clim. Past Discuss., https://doi.org/10.5194/cp-2018-157
Manuscript under review for journal Clim. Past
Discussion started: 7 December 2018

Pacific, (3) the results are easily compared to earlier observations at other cores and drill sites, and (4) the large changes of $CaCO_3$ produce the characteristic seismic horizons found in the eastern Pacific (Mayer et al, 1986; Bloomer and Mayer, 1997). We then use MARs and other elemental data to understand the causes of each PPLC. Both high relative production of biogenic opal (a dilutant) and high dissolution of $CaCO_3$ (carbonate removal before burial) have contributed to low $CaCO_3$ intervals.

5.1 Low $CaCO_3$ % Intervals in the Pliocene and Pleistocene

Two primary factors cause low $CaCO_3$ intervals—excess opal production and/or higher than average relative $CaCO_3$ dissolution. The late Miocene and early Pliocene have high $CaCO_3$ variability in the LMBB interval largely driven by variability in relative opal and $CaCO_3$ production. Low $CaCO_3$ intervals are coherent through all 7 records and have lowest $CaCO_3$ in deeper sites away from the highest productivity. Such coherence is indicative of a region-wide high $CaCO_3$ dissolution at the sea floor superimposed upon depth-dependent $CaCO_3$ dissolution, in addition to the latitudinal $CaCO_3$ production gradient characteristic of the equatorial Pacific (Honjo et al, 1995). In Table 2 and Figure 4 we have defined five PPLCs. The same low carbonate intervals can also be found in the low-resolution profiles of DSDP Sites 572 and 573 from Farrell and Prell (1991), although the timing of the older low $CaCO_3$ intervals are shifted in age because of defects in the earlier age models. The lowest $CaCO_3$ % occurs at about 4 Ma (Figure 4, PPLC-4C, 3834-4093 ka), and since that time $CaCO_3$% has slowly climbed to peak at about 500 ka, just before the initiation of PPLC-1.

The ~100 kyr $CaCO_3$ variation (Hays et al, 1969; Farrell et al, 1989; Murray et al, 2000) characteristic of the Pleistocene equatorial Pacific dominates the $CaCO_3$% records between 0 and 1.9 Ma, but the older record has much more long period variability (≥400 ka). $CaCO_3$ % is high in Pleistocene glacial climate intervals and is low in interglacials. Development of ~100-kyr cyclicity in the carbonate record predates the development of 100-kyr periodicity in the oxygen isotope record by about 1 Myr. The 100-kyr $CaCO_3$ cycles are discussed further in section 6.2

5.2 Potential sediment focusing at U1337

$CaCO_3$ MAR records are similar throughout the eastern equatorial Pacific, indicating that much of the variability in an individual record is caused by regional factors, not local sedimentation processes (Figure 5). However, Site U1337 has anomalous deposition that is evidence for strong local sediment focusing (Francois et al, 2004; Lyle et al, 2005a; Tominaga et al., 2011; Marcantonio et al, 2014). Most of the drill sites in this paper have variability in the bulk sediment MAR, but most of the bulk MAR variation is typically derived from changes $CaCO_3$ MAR. Site U1337 is unique because it clearly has much higher (non-$CaCO_3$) opal and clay deposition unrelated to $CaCO_3$ burial. The highest anomaly occurs between about 4.5 and 3 Ma, and a secondary anomaly occurs between 6.2 and 5.4 Ma. The two intervals may have higher than average deep current activity to focus the sediments to Site U1337. We propose that deposition at Site U1337 is the result of local sediment focusing adding fine sediments to the sediment column at the drill site (Marcantonio et al, 2014; Lyle et al, 2014;

Clim. Past Discuss., https://doi.org/10.5194/cp-2018-157
Manuscript under review for journal Clim. Past
Discussion started: 7 December 2018

Lovely et al, 2017). When currents are moderate in strength, sediment focusing preferentially moves the fine fraction of sediments (Lyle et al, 2014; Lovely et al, 2017) as is observed in the Site U1337 record. In addition, seismic profiles and bottom bathymetry have shown active erosional channels around the northern and eastern edges of the Site U1337 survey area (Figure SM-1b, Supplemental Material; Pälike et al., 2010).

Surprisingly, the sediment focusing at Site U1337 does not strongly affect the $CaCO_3$ % profile, but does result in anomalously high sedimentation rates, lower average $CaCO_3$ contents, and higher than expected $CaCO_3$ MAR. For example, average $CaCO_3$ % for Site U1337 is 39.5% versus 54.5% for U1335, despite Site U1335 being 1.5° further north and further away from equatorial production. Similarly, $CaCO_3$ MAR at Site U1337 averages 20% higher than the $CaCO_3$ MAR at Site U1338 for the last 8 Myr despite being further from the equator than Site U1338.

5.3 High production intervals: PPLC 5 (4465 to 4737 ka) and PPLC 2 (1685 to 2135 ka)

High biogenic opal production during Pliocene and Pleistocene diatom deposition intervals can be distinguished by (1) low $CaCO_3$ content, presumably by dilution with diatom opal, (2) little change in clay MAR but large change in opal content and opal MAR, (3) increase or little change in $CaCO_3$ MAR, and (4) lowest $CaCO_3$ % at sites closest to the equatorial upwelling zone. Sites away from the equator may actually have higher $CaCO_3$% in the diatom deposition interval presumably because of increased production by calcareous nannofossils relative to time intervals on either side. The low $CaCO_3$ near the equator is caused mostly by dilution of $CaCO_3$ by high fluxes of biogenic opal to the sea floor. With a proper age model and with XRF scanning data it is possible to distinguish a $CaCO_3$ low caused by elevated opal production from intervals caused by higher $CaCO_3$ dissolution at the sea floor.

PPLC-5 (4737-4465 ka) is the youngest of the diatom deposition intervals associated with the LMBB and exhibits all the characteristics of a high production interval. Sites 849 and 850, sites straddling the equator at 5 Ma (Table 1), exhibit a pronounced $CaCO_3$ % low at this time (Figure 4), but sites farther away from the equator exhibit much smaller $CaCO_3$ % change (Sites 848, 851, and U1338) or even slight $CaCO_3$ % increases (Sites U1337, U1335). All sites have relatively high or unchanged $CaCO_3$ MAR within PPLC 5 (Figure 5). Opal data is only available for Sites 849, U1338, and U1337, and the records exhibit a large opal MAR peak at Site 849, a small peak at Site U1338, and ambiguous change at Site U1337, exacerbated by potential sediment focusing there.

PPLC-2 (2135-1685 ka) is found at the equator at Site 849, but is also found at Site U1338. We infer that there was higher opal deposition at Sites 848 and 850 because of the low $CaCO_3$ content. The equivalent of the PPLC-2 interval has also been reported to the east of the Galapagos Islands (Sites 846 and 847, Farrell et al, 1995; Site 846, Lawrence et al., 2006; Site 1240, Povea et al., 2016). There are clear opal MAR peaks at Site 849 (Figure 6) that match in time and magnitude with a similar interval from Site 1240 (Povea et al, 2016). Major opal MAR highs within PPLC-2 align with glacial intervals in the

Clim. Past Discuss., https://doi.org/10.5194/cp-2018-157
Manuscript under review for journal Clim. Past
Discussion started: 7 December 2018

oxygen isotope series between MIS 78 and MIS 60, even though the highest opal MAR is in an interglacial (MIS 75). $CaCO_3$ % lows within PPLC-2 don't always align with high opal MAR, indicating $CaCO_3$ dissolution has also occurred. At Site U1338, low $CaCO_3$% and highest opal MAR are not aligned, evidence that a dissolution overprint exists.

5.4 Early Pliocene extensive $CaCO_3$ dissolution: PPLC-4 (4093-2915 ka)

Immediately after the LMBB ends there is the PPLC-4 interval of very low $CaCO_3$ %. The minimum is found throughout the eastern and central equatorial Pacific west of the East Pacific Rise The base of PPLC-4 constitutes the acoustic impedance contrast that causes the Pliocene 'green' seismic horizon (Mayer et al, 1986; Bloomer et al, 1997). At Site 850, Bloomer and Mayer (1997) identified a series of seismic horizons that can be linked to the $CaCO_3$ variability associated with PPLC-3, 4, and 5.

PPLC-4 is made up of 3 low $CaCO_3$ % intervals between 2915 and 4093 ka (Table 2) with lower $CaCO_3$ % and more consistently low $CaCO_3$ % at sites further away from the equator. The lowest $CaCO_3$ % in all the records is found at U1337 between 4500 and 3500 ka because of extensive clay and opal dilution from apparent sediment focusing in addition to $CaCO_3$ % dissolution (Figures 4 and 5). Nevertheless, relatively shallow sites along the Leg 138 transect also exhibit coherent $CaCO_3$ change, as exhibited by the standardized $CaCO_3$ % records (Figure 4, lowest record). The low bulk MAR and $CaCO_3$ MAR over the PPLC-4 interval indicates that dissolution was a major factor shaping the $CaCO_3$ record. The PPLC-4 set of dissolution-induced $CaCO_3$ % lows occurs at an important juxtaposition of tectonic and environmental influences. Slow closure of the Central American Seaway was severing connections between the Caribbean and Pacific. However, extensive changes were also going on in global climate, so it is currently impossible to isolate the seaway closure effect from other changes in the eastern Pacific (Molnar, 2008; O'Dea et al, 2016; Molnar, 2017).

5.5 PPLC-3 (2684-2248 ka): $CaCO_3$ dissolution at the initiation of Northern Hemisphere glaciation:

PPLC-3 consists of two dissolution intervals separated by a distinctive high $CaCO_3$% triplet. PPLC-3 can best be seen in the stacked and standardized $CaCO_3$ % profile (Figure 4, bottom). They also can be found at Site 573/574 (Farrell et al, 1991). The consistent expression of these $CaCO_3$ % lows merited their inclusion in this list. Deeper sites within the eastern Pacific have prominent lows around the triplet of high $CaCO_3$ %, while records from the shallower Leg 138 sites have weaker variability. Along the relatively shallow Leg 138 transect (~3800 m water depth) PPLC-3 lows are most pronounced south of the equator at Site 848 (3°S) and north of the equator at Site 851 (2.7°N), as expected if dissolution is superimposed upon an equatorial maximum of $CaCO_3$ production. The timing of PPLC-3 suggests an association with the initiation of northern hemisphere glaciation, or at least with changes in abyssal circulation at that time.

Dissolution at PPLC-3 can be shown by the $CaCO_3$:$BaSO_4$ ratio (Figure 7). Lyle and Baldauf (2015) proposed that the $CaCO_3$:$BaSO_4$ ratio is a good measure of relative preservation, since $CaCO_3$ preservation is highly variable, but Ba preservation is relatively constant (Dymond et al, 1992; Balakrishnan Nair et al, 2005). In addition, particulate Ba rain

Clim. Past Discuss., https://doi.org/10.5194/cp-2018-157
Manuscript under review for journal Clim. Past
Discussion started: 7 December 2018

caught in sediment traps is proportional to the C_{org} rain, so normalizing to Ba largely normalizes out the production variability and leaves a signal dominated by $CaCO_3$ dissolution. Highest $CaCO_3$:$BaSO_4$ ratios in the XRF data set are found at Site 849, which is shallower and has about twice the sedimentation rate of Site U1338 or U1337 (Table 2). As expected, the ratio indicates lower dissolution while compensating for the higher production at Site 849. The records also clearly show the dissolution signals in PPLC-4 as well as PPLC-3. The $CaCO_3$:$BaSO_4$ ratio around PPLC-3 clearly shows similar responses in all the records where Ba data is available, with two low $CaCO_3$ intervals surrounding the $CaCO_3$ % high (Figure 7).

5.5 PPLC-1: low $CaCO_3$ interval among the 100-kyr Pleistocene cycles

The PPLC-1 interval is superimposed upon the classic Pleistocene Pacific100-kyr glacial carbonate cycles (Figure 7). Significant 100-kyr $CaCO_3$ cyclicity first appears at about 1900 ka in the eastern Pacific, well before appearance of 100-kyr benthic oxygen isotope cycles at ~900 ka that define the Mid-Pleistocene Transition. If Sites U1338 and 849 are compared it is clear that dissolution is a major factor in the cycles. Site 849 has much higher $CaCO_3$:$BaSO_4$ (less dissolution) than the other sites and much weaker 100 kyr cycles, suggesting that dissolution is shaping the Site U1337 and Site U1338 record. Not only does dissolution increase the 100-kyr cycle amplitude but also selectively removes higher frequency changes in the $CaCO_3$:$BaSO_4$ ratio that are apparent at Site 849. Highest $CaCO_3$ preservation as well as highest $CaCO_3$ % occurs just before the beginning of PPLC-1. The time offset of the low $CaCO_3$:$BaSO_4$ ratio at Site 849 results from relatively weak dissolution in the early part of PPLC-1. These cycles largely match the CCD changes found by Farrell and Prell (1989) at around 140°W.

6. Discussion

Reconnaissance paleoceanographic descriptions of the Cenozoic equatorial Pacific (van Andel et al, 1975; Berger, 1973) often gloss over the late Miocene and early Pliocene as being periods almost like the present. The CCD variability within the last 12 million years is not nearly as dramatic as the huge changes earlier in the Cenozoic (Pälike et al, 2012). Nevertheless, as more detail has been generated from better chronology and additional regional records, significant changes can be found throughout the equatorial Pacific since 12 Ma. Variability in the late Miocene and afterward represent profound changes in how $CaCO_3$ has been produced and recycled within the Pacific.

Two major processes affect carbonate burial in the equatorial Pacific—high production within the surface waters of the equatorial productivity belt may increase $CaCO_3$ rain but dilute $CaCO_3$ sediment concentrations with bio-SiO_2 (opal), while dissolution by DIC-rich deep waters from the North Pacific may reduce $CaCO_3$ burial by increased $CaCO_3$ dissolution at the sea floor. $CaCO_3$ burial is the net difference between biogenic $CaCO_3$ production and dissolution at the sea floor. Dissolution

Clim. Past Discuss., https://doi.org/10.5194/cp-2018-157
Manuscript under review for journal Clim. Past
Discussion started: 7 December 2018

effects can be distinguished from those caused by productivity, in particular, dilution by high biogenic opal deposition, by using burial fluxes (MAR) along with other sediment chemical data.

The CCD concept is most useful at a reconnaissance scale. Using a ratio such as $CaCO_3$:$BaSO_4$ to normalize for different $CaCO_3$ rain rates provides the best indicator of relative dissolution at any given drill site (Figure 7). We find that dissolution is most pronounced in the early Pliocene (PPLC-4) and is evidence that a major reorganization of carbon storage in the Pacific occurred then. We also found that opal dilution shapes the record, especially in PPLC-5 and PPLC-2. More XRF data, especially from ODP Leg 138 and ODP Leg 202 would be very useful to better understand the Pacific carbon cycle.

6.1 Changes in depth dependent dissolution: eastern equatorial Pacific CCD

The CCD is a common metric for variations in carbon cycle over time. Unfortunately, changes in the CCD can be difficult to interpret because changes in $CaCO_3$ production affect the CCD just as strongly as variations of abyssal dissolution. The early discussions of the Pacific CCD, for example, found that the depth to complete $CaCO_3$ dissolution was deeper under regions of higher $CaCO_3$ production at the equator (Berger, 1973; van Andel and Moore, 1974). Without regional drill sites that span the CCD within the same production regime it remains difficult to define CCD changes except in low resolution or for abrupt large CCD movements like at the Eocene-Oligocene boundary (Coxall et al, 2005; Pälike et al, 2012).

Lyle et al (2005b) used the gradient in $CaCO_3$ MAR with depth between drill sites to define changes in the Eocene CCD. Depth is corrected for crustal cooling and sediment loading. Working backwards from $CaCO_3$ burial (MAR) has many ambiguities, however, and local sedimentation anomalies at the drill sites used cause significant noise. For large changes as in the Eocene, the $CaCO_3$ MAR gradient approach works, but the weaker signal in the Pliocene and Pleistocene is harder to distinguish from the noise.

$CaCO_3$ MAR at any given location and time can be represented as a combination of the net focusing, rain, and dissolution as in equation (1):

$$CaCO_3\ MAR_T = F_T\,(CaCO_3\ rain_T) - D_T \quad (1)$$

where the T subscript refers to time T, rain refers to the particulate $CaCO_3$ arriving at the bottom from surface $CaCO_3$ production, F is the sediment focusing factor, and D is the $CaCO_3$ dissolution at the sea floor. The variation of D responds to the chemistry of the regional water mass and depth of the sea floor; but regional variability is typically a depth function because of the large spatial scale of deep water masses. However, sediment focusing is locally variable and $CaCO_3$ production typically has a much smaller spatial scale than water masses that control dissolution. Production and sediment focusing are thus difficult to control for in order to get the dissolution component.

Clim. Past Discuss., https://doi.org/10.5194/cp-2018-157
Manuscript under review for journal Clim. Past
Discussion started: 7 December 2018

Two of the sites in this study (Site 851 and Site U1338) are now at roughly the same latitude and have similar modern particulate organic carbon standing stock from satellite estimates (58 mg/m^3 POC at Site 851; 57 mg/m^3 POC at Site U1338, NASA Goddard Space Flight Center, 2014). Hypothetically, if relative sediment focusing at both sites remained constant, the gradient in $CaCO_3$ MAR should extrapolate to zero $CaCO_3$ flux at the CCD. Relative sediment focusing over long time frames in the pelagic regime appears reasonably constant (Liao and Lyle, 2014; Mitchell and Huthnance, 2013), and current-related anomalies can be discerned from the seismic profiles from site surveys. Sites chosen for drilling were chosen for the lack of anomalous seismic character in both ODP Leg 138 and IODP Exp 320/321. The $CaCO_3$ MAR gradient using Sites 851 and U1338 is noisy but that general trends can be discerned (Fig 5). The trends are consistent with trends in $CaCO_3$ MAR and $CaCO_3$:$BaSO_4$ as indicators of enhanced dissolution.

The CCD estimate using $CaCO_3$ MAR appears noisy over longer time frames because of a combination of relatively high frequency changes (e.g., the 100-kyr cycles in the last million years) but also suffers from the noise resulting from building the trend with records from only 2 sites. Minor errors in correlation plus local changes in $CaCO_3$ production or burial are magnified in the CCD estimate. For example, Site U1338 occasionally had higher $CaCO_3$ MAR than Site 851, making for a negative CCD gradient with depth. Negative trends result from either $CaCO_3$ production anomalies relative to modern conditions or changes in sediment focusing. These intervals were removed from the CCD estimate (e.g., the gap in the record between 2000 and 2500 ka).

Two levels of smoothing are used in Fig 5, 50 kyr and 750 kyr. The shorter time frame is adequate to show higher resolution changes, while the latter captures the longer trends. It is clear from these records that the late Miocene-Recent CCD has been strongly affected by changes in production. The LMBB interval has the deepest CCD since 8 Ma as well as the highest $CaCO_3$ MAR at both Sites U1338 and 851. It is likely that higher $CaCO_3$ production over Sites 851 and U1338 drove the eastern Pacific CCD deeper during this interval.

The CCD starts to shallow beginning at ~4800 ka, as the LMBB was fading. The shallowest CCD determinations do not precisely align with the PPLC-4 intervals although PPLC-4 is contained within a broad CCD minimum, indicating both a response to lowered $CaCO_3$ deposition and as indicated by $CaCO_3$:$BaSO_4$, to increased dissolution. During PPLC-1, the low $CaCO_3$% is clearly averaged over broad variability in $CaCO_3$ dissolution. Nevertheless, low $CaCO_3$:$BaSO_4$ during the PPLC-1, 3 and 4 intervals also indicate that enhanced dissolution was an important factor in the low average $CaCO_3$% (Figure 7).

$CaCO_3$:$BaSO_4$ ratios from XRF scanning provides an alternative way to investigate changes in dissolution before burial. Advantages of this approach are that relative dissolution can be assessed at a single location and can also be compared regionally. $BaSO_4$ is produced as a result of particulate organic carbon (POC) rain, and Ba is much more consistently preserved during sediment burial (Dymond et al, 1992; Griffith and Paytan, 2012). Both bio-Ba and $CaCO_3$ rain are well-

Clim. Past Discuss., https://doi.org/10.5194/cp-2018-157
Manuscript under review for journal Clim. Past
Discussion started: 7 December 2018

correlated to POC production (Dymond and Collier, 1996), so changes in the $CaCO_3$:$BaSO_4$ ratio primarily mark changes in the relative preservation of $CaCO_3$ (Lyle and Baldauf, 2015). Across the sites where XRF scanning data are available, there is common signal that indicates strong dissolution within PPLC-3 and PPLC-4 (Figure 7).

Scaling the data by standard deviations better illustrates the common signal among all the sites where Ba data is available (Figure 7b). The PPLC-3 and PPLC-4 intervals clearly have lower average $CaCO_3$:$BaSO_4$ at the four drill sites with XRF data. These sites span from the equator to more than 5°N and are up to 1900 km apart. The common dissolution record thus covers a significant portion of the east-central Pacific. Lowest $CaCO_3$:$BaSO_4$ ratios are found in PPLC-4c and -4a, also shown by lower $CaCO_3$ MAR than in other intervals (Fig 5). $BaSO_4$ MAR during PPLC-4c and -4a are relatively high, so dissolution must have outpaced somewhat higher $CaCO_3$ production relative to stratigraphic intervals on either side (See Supplemental Tables SM-17 to SM-21). The difference between the CCD change and the $CaCO_3$:$BaSO_4$ probably results from the added $CaCO_3$ rain within PPLC-4.

The dissolution anomalies cover a large regional extent as expected from the large regional extent of deep water masses. PPLC-3a and -3b are very consistent across the set of drill sites, and mark dissolution on either side of a distinctive $CaCO_3$:$BaSO_4$ maximum all occurring as the northern hemisphere glaciations began.

6.2 Early beginnings of Pleistocene 100-kyr $CaCO_3$ cyclicity

Both the $CaCO_3$ % and the $CaCO_3$:$BaSO_4$ records illustrate the development of 100-kyr dissolution cyclicity in deep Pacific dissolution. Surprisingly, the 100-kyr dissolution cyclicity began significantly before the mid-Pleistocene transition at ~900 ka, at which time 100-kyr benthic oxygen isotope cycles became prominent. The dissolution cycles isolated by $CaCO_3$:$BaSO_4$ begin at about 1900 ka (Figure 8a) and build in amplitude until MIS 16 at 655 ka. High $CaCO_3$ preservation is associated with periods of higher ice volume since about 1700 ka (MIS 58).

The appearance of 100-kyr power can also be tracked via wavelet time series of the stacked $CaCO_3$:$BaSO_4$ record (Figure 8b). Strong power is found at 100 kyr from 1900 ka going forward in time and in the brief interval between PPLC-3a and -3b. Relatively strong 41-kyr power ka is also apparent associated with the 100-kyr cycles since 1900 ka, and strong 41-kyr power is found at the end of the LMBB.

The early appearance of 100-kyr $CaCO_3$ dissolution cycles in the equatorial Pacific is interesting but problematic. There is a tendency even within the $\delta^{18}O$ 41kyr world for high $CaCO_3$ preservation to be associated with periods of heavier than average oxygen isotope cycles, and presumably cooler high latitude regions. Figure 8a compares the $CaCO_3$:$BaSO_4$ combined stack, where a high value indicates better $CaCO_3$ preservation, to the combined Site 849-Site U1338 isotope record. Figure 8a also has a smoothed record of the oxygen isotope values, to illustrate the low-frequency dips in the isotope record in the earlier part of the record.

Clim. Past Discuss., https://doi.org/10.5194/cp-2018-157
Manuscript under review for journal Clim. Past
Discussion started: 7 December 2018

When both oxygen isotopes and $CaCO_3$:$BaSO_4$ have strong 100-kyr cycles (1000-0 ka), it is very clear that high $CaCO_3$ preservation is associated with cold, heavy isotope intervals. In the interval from 1000-1650 ka (MIS 25-59), the correlation is still strong when $CaCO_3$:$BaSO_4$ is compared to the smoothed oxygen isotope record. The correlation is weaker before 1600 ka, but between 2400 and 2600 ka the high $CaCO_3$ preservation interval between PPLC-3a and -3b is also characterized by a heavy oxygen isotope signal.

The 100-kyr $CaCO_3$ cycles that appear in the Pacific could also appear in the deep Atlantic if there is cyclic weathering or NADW formation. Unfortunately there are few $CaCO_3$ records for the Atlantic Ocean over the period between 1 and 2 Ma. Ruddiman et al (1989) have a $CaCO_3$ profile from Site 607, at a depth of 3426 mbsl. Because it is shallow relative to AABW in the Atlantic, it is unlikely to be affected by dissolution and instead appears to be affected by changes in clay deposition over glacial-interglacial cycles (Broecker and Turekian, 1971; Bacon, 1984). The $CaCO_3$ % record at 607 changes from 41-kyr cyclicity to 100-kyr cyclicity at ~900 kyr, like the $\delta^{18}O$ record. Harris et al (1997) developed a $CaCO_3$ dissolution index for the Ceara Rise and found that dissolution affected the $CaCO_3$ records below a depth of 4356 mbsl. The index compared $CaCO_3$ MARs at the deep Site 929 to the shallow Site 925, and found coherence with the oxygen isotope record of ice volume for the last million years. However, 100-kyr coherence was not very strong in the 1-2 Ma period. Since the dissolution record at the Ceara Rise primarily reflects oscillations in the penetration of AABW vs NADW around Ceara Rise, changes in NADW flow do not cause the Pacific oscillation. The differences between the Atlantic and Pacific $CaCO_3$ records imply the development of oscillations in deep storage of DIC in the Pacific, but little communication of this oscillation between ocean basins before the 900 ka mid-Pleistocene climate transition. The lack of strong cycles at the Ceara Rise may actually be caused by relatively strong NADW formation in the Atlantic prior to 1 Ma and the development of NADW production cycles only after the mid-Pleistocene climate transition (Kleiven et al., 2003).

For the 2.6 million years of the Pleistocene we observe an important linkage between $CaCO_3$ preservation and higher ice volume. Farrell and Prell (1989) have argued for a change in carbonate ion concentration variability of about 6% to drive the glacial-interglacial cycles since 800 ka. Hodell et al. (2001) have argued that the Indo-Pacific association of high $CaCO_3$ burial with glacials is evidence for cycles driven by shelf-basin fractionation of carbonate burial. During high sea level stands, the additional burial of $CaCO_3$ on shallow tropical shelves reduces deep $CaCO_3$ burial, while exposure of these shelves during glacials transfers $CaCO_3$ burial to the deep ocean and also consumes atmospheric CO_2 through carbonate weathering. The correlation that we observe between higher $CaCO_3$:$BaSO_4$ and heavy oxygen isotopes is supportive of a primary control of deep $CaCO_3$ burial by shelf-basin transfer through the Pleistocene, with ocean circulation transferring the signal mostly to the Pacific.

Clim. Past Discuss., https://doi.org/10.5194/cp-2018-157
Manuscript under review for journal Clim. Past
Discussion started: 7 December 2018

6.3 Origins of PPLC-4 and the Pliocene temperature maximum

Pleistocene changes in dissolution are adequately explained by shelf-basin fractionation, but the Pliocene PPLC-4 dissolution series requires more. Most of PPLC-4 is associated with lower frequency dissolution variability prior to 2600 ka (Fig 7, Fig 8) and the PPLC-4 intervals are also marked by extreme lows in $CaCO_3$ MAR (Fig 5).

The timing of PPLC-4 occurs during the final closure of the Central American Seaway (O'Dea et al, 2016) that implies that the closure and the extreme dissolution are somehow linked. Bell et al (2015) suggest that NADW formation was strong prior to isotope evidence of Panama Seaway closure and largely unaffected by changes associated with the Panama Seaway closure. Furthermore, they propose that the circulation effects of closure developed prior to 4 Ma.

Poore et al (2006) have proposed that the deep sill at the Greenland-Scotia Ridge between 6000 and 2000 ka caused a radical increase in volume of NCW production, as estimated by $\delta^{13}C$ gradients between the North Atlantic-Southern Ocean-Pacific. Such an increase should increase basin-basin fractionation of $CaCO_3$ burial between the Atlantic and Pacific. However, PPLC-4 also occurs immediately after the end of the LMBB, marking a major drop in biogenic $CaCO_3$ rain regionally in the Pacific, and is also a period of high estimated atmospheric CO_2 (Seki et al, 2010; Stap et al, 2016). PPLC-4 occurs during an interval of warm tropical SST after the SST minimum at 5.4 Ma (Herbert et al., 2016). In other words, attributing PPLC-4 to one cause is overly simplistic.

Nevertheless, it is possible to say that during the early Pliocene the Atlantic was preferentially flushed of DIC, making a strong $\delta^{13}C$ gradient from Atlantic to Pacific. Between 4 and 2.5 Ma, however, the gradient between Atlantic and Pacific gradually weakened (Fig 9), indicating buildup of low ^{13}C waters in the Antarctic-controlled deep circulation. The global SST warm transient between ~5.4 to 3 Ma (Herbert et al, 2016), as well as the elevated CO_2 suggests an important perturbation of the carbon cycle. At Site 1241 on the Cocos Ridge northeast of the sites in this paper, records of temperature and biogenic MAR find the interval between 5.4 and 3 Ma to be unusually warm but with relatively low biogenic production when compared to the LMBB (Seki et al., 2012).

The movement of the equatorial Pacific locus of high biogenic deposition from the east central equatorial Pacific to the eastern Pacific (Fig 1; Farrell et al, 1995; Lawrence et al, 2006) may have triggered PPLC-4, by removing $CaCO_3$ rain from the region west of the Galapagos Islands that had up until then compensated for the elevated dissolution at the sea floor. However, low $CaCO_3$ MAR apparently marks the PPLC-4 interval in the easternmost Pacific as well (Sites 846 and 847, Farrell et al, 1995) and gives evidence that moving the locus of production is not the primary cause for PPLC-4.

Bell et al (2015) have given a good summary of stable isotopes in the Atlantic and far South Atlantic, which they compared to Site 849. Sites U1338 and U1337 have virtually the same $\delta^{13}C$ signature as Site 849 (Drury et al, 2016, 2017; Tian et al,

2018) so Site 849 represents an east-central Pacific deep water signal. The $\delta^{13}C$ time series in the Pacific is nearly flat between 5 and 2 Ma (Fig 9). During the period between 4.4 and 4.2 Ma, the southernmost South Atlantic sites (Site 704) became isotopically heavier and more like the North Atlantic, and were interpreted to indicate deep expansion of the NADW tongue and somewhat stronger NADW flow during the warm Pliocene (Hodell and Venz-Curtis, 2006; Bell et al., 2015). After 4 Ma, the Atlantic profile at Ceara Rise became isotopically lighter while the Pacific profiles got somewhat heavier, evidence for expansion of an Antarctic source that penetrated more effectively into both the Atlantic and Pacific. Similarly, Nd isotopes and Cd/Ca on Walvis Ridge find an Antarctic end member signal that reached a local minimum around 3.5- 4 Ma (Klevenz et al, 2008) and concluded that NADW flow was highest then. We suggest that the more thorough exchange of Pacific deep water after 3.5 Ma helped to increase deep dissolution in the Atlantic and enhanced Atlantic 100-kyr cyclicity that was beginning to occur in the Pacific. .

In the absence of conclusive evidence, we suggest that the enhanced dissolution in PPLC-4 marks the effects of enhanced Antarctic flow within the deep Pacific and a larger reservoir of low $[CO_3]^=$ water in the deep ocean between 4.1 and 2.9 Ma. Sites U1337, U1338, and Site 849 all are sites within the mixing zone of Pacific deep water outflow with relatively weak deep flow from the Antarctic, at least compared to the western Pacific. The lack of strong change of $\delta^{13}C$ despite apparent increases in Antarctic influence worldwide, suggests continued deep DIC storage in the Pacific. Since the period between 5 and 3.5 Ma was also warm (Herbert et al, 2016), there may also be feedbacks from the carbon cycle as well as enhanced shelf storage of $CaCO_3$ from high sea levels reducing deep $CaCO_3$ burial. However, sea levels were relatively high for millions of years prior to the 4-3 Ma period of PPLC-4 (Rohling et al, 2014; Miller et al, 2005), so the sea level effect should not have been large.

6.4 The PPLC-5 and PPLC-2 high production intervals

One of the major features within sediments of the eastern Pacific is a series of high biogenic sediment deposition intervals in the late Miocene (the LMBB, including PPLC-5) as well as a significant interval at 2000 ka that is strongest in the eastern Pacific (PPLC-2). Apparently conditions conducive to high primary production were put in place for hundreds of thousands of years (Table 2). Detailed analyses of the causes of the production intervals are beyond the scope of this paper, but here we will describe future research directions.

The LMBB has multiple intervals of high biogenic deposition after 8000 ka (Figures 4 and 5; Farrell et al, 1995; Lyle and Baldauf, 2015), ending with PPLC-5. The cause of the variability needs further investigation. Many regions worldwide have intervals of high production, which may have a common cause. Globally, high biogenic deposition in the Indian Ocean, North Pacific, and the Benguela upwelling zone define a proposed global late Miocene production interval (Farrell et al, 1995; Filippelli, 1997; Dickens and Owen, 1999; Diester-Haass et al., 2002; Grant and Dickens, 2002).

Clim. Past Discuss., https://doi.org/10.5194/cp-2018-157
Manuscript under review for journal Clim. Past
Discussion started: 7 December 2018

Many drill sites exhibit increased biogenic burial within the late Miocene, but the timing varies significantly between regions. Dickens and Owen (1999) propose that upwelling in the Indian Ocean was high between 9 and 3.5 Ma but most intense between 6 and 5 Ma. Dickens and Barron (1997) recognized an interval of high pennate diatom deposition between 5.0 and 5.9 Ma in the subarctic North Pacific and noted that the timing matched pennate diatom layer deposition in the equatorial Pacific (Kemp and Baldauf, 1993). Highest biogenic deposition in the Benguela current region also occurred in the period between 7 and 4.5 Ma (Diester-Haass et al, 2002). Within the Exp 320/321 sites and the ODP Leg 138 sites along the 110°W transect, there is also high but variable biogenic MAR between around 7.5 Ma and the end of PPLC-5 at 4.47 Ma that indicate high primary production. Typically the highest biogenic deposition was between 7 and 6.5 Ma. Broadly in the late Miocene, especially after 7.5 Ma, it is common to find high biogenic sediment deposition and presumably high primary production.

Hypotheses to the cause of high primary productivity vary. Filipelli (1997) proposed that the uplift of the Himalayas (Molnar et al., 1993) and late Miocene intensification of the Asian Monsoon caused higher weathering and larger transport of nutrients to the oceans. Diester-Haass et al (2002) suggested that reorganization of ocean circulation is likely to have played an important role, as well as intensification of trade winds.

Higher biogenic deposition within the equatorial Pacific broadly occurred within the late Miocene but also extends through the Pliocene in the easternmost equatorial Pacific (Figure 10). Million year increments of $CaCO_3$ MAR and noncarbonate (mostly biogenic opal) MAR are shown from drill sites in the equatorial zone from near the 81°W longitude of the coast of Ecuador to almost 120°W, halfway to Hawaii. For all but the easternmost part of the equatorial transect high $CaCO_3$ MAR is confined within the time frame of the LMBB. However, east of about 100°W on the Nazca Plate, the opal deposition is much higher in the Pliocene and Pleistocene, as shown by the increased noncarbonate MAR post-LMBB.

A similar lack of a common pattern is found worldwide. Highest deposition in the equatorial Pacific LMBB is in the region near the equator between about 108°W and 126°W (Fig 1), and the highest MAR was at the beginning of the LMBB, around 7 Ma. Within the Benguela Current Site 1085 has highest biogenic MAR at the end of the LMBB interval (Diester-Haass etal, 2002). Peak diatom deposition in the subarctic North Pacific occurred in the middle of the LMBB interval, between 6 and 5 Ma (Dickens and Owen, 1999; Dickens and Barron, 1997). And, in the California current region, diatom deposition decreased offshore at the beginning of the LMBB (7.5 Ma) to become more confined to the coastal region, implying decreased overall deposition (Barron et al., 2002).

Farrell et al (1995) described the abrupt drop in biogenic deposition along the 110°W transect at the end of the LMBB but continued high deposition to the east. They proposed that the change was related to movement of biogenic depocenters resulting from CAS closure. Sites drilled on the Carnegie Ridge by ODP Leg 202 support a major increase in biogenic

sedimentation in the east associated during the time of CAS closure (Fig 10). Both Sites 1238 and 1239, near Ecuador, are situated on crust formed in the late early Miocene. Both essentially have a hiatus until ~8 Ma (ODP Leg 202 Shipboard Scientists, 2003). Biogenic sedimentation at both Sites 1238 and 1239 rapidly increased after 7 Ma, peaked between 3 and 5 Ma, and continued to remain high up to the Holocene. Apparently the easternmost Pacific became more productive because of the formation of the Isthmus of Panama. Nevertheless, high levels of paleoproductivity found after 8 Ma worldwide suggest that regional production intervals are superimposed upon a global signal. Now that high-resolution records of biogenic deposition are available from the east-central Pacific, there is a need to revisit the timing of regional changes in biogenic deposition through the late Miocene.

When the LMBB and PPLC-2 are examined in detail in the equatorial Pacific, we find that the dynamics of nutrient delivery to the equatorial Pacific cannot be ignored. Figure 6 shows PPLC-2 within Site 849, and is comparable to Site 1240 in the Panama Basin (Povea et al, 2016) and Site 846 (Lawrence et al, 2006). There is clearly an orbital periodicity at Site 849, as well as depositional events on the <1 kyr resolution of the XRF record.

Similarly, within the LMBB at the XRF-scanned intervals of Site U1338 and Site 849 there is high opal variability on the millennial scale based upon the XRF estimated opal:clay ratio, suggesting that long opal deposition intervals are made up of large numbers of individual opal deposition events. These deposition intervals correlate to the intervals where diatom mats have been found in the equatorial Pacific cores, around 4.2 Ma, 5.5 Ma, and 7.3 Ma (Figure F23, Pälike et al, 2010b; Kemp and Baldauf, 1993). As a side note, we do not find elevated clay deposition within the LMBB (Fig 4), so the elevated biogenic MARs do not result from higher dust fertilization but instead seems to result from interoceanic reorganization of nutrient inventories (Ziegler et al, 2008).

High productivity intervals in the eastern Pacific result from a combination of factors. There appears to be elevated production globally within the LMBB, for example, indicating higher availability of nutrients in surface waters generally in the late Miocene. However, timing of intervals of high productivity depends on how the nutrients flow to different upwelling regions, and provide insight into how the sub-surface oceans have changed. The appearance of PPLC-2 and its stronger expression to the east of our study (Lawrence et al, 2006; Povea et al, 2016), show that long intervals of better connection to nutrients have occurred well into the Pleistocene.

7 Conclusions

We have used XRF scanning and new age models to create records of bulk sediment chemistry and MAR to 8.3 Ma for Sites U1335, U1337, and U1338 from Exp 320/321, and to 7.2 Ma at Site 849 from ODP Leg 138. We have also used the sediment bulk density-$CaCO_3$ relationship and stratigraphic correlation to dated cores to create 0-8.3 Ma $CaCO_3$ % and

$CaCO_3$ MAR records from Sites 848, 850, and 851. In this paper we have described these records after the Miocene-Pliocene transition. The seven sites have a common high-resolution stratigraphy that should allow important further work regionally.

With bulk chemical data and a geographic range of drill sites it is possible to distinguish between dissolution and production as causes of low $CaCO_3$ intervals in the Pliocene-Pleistocene record. We identified five long-term low $CaCO_3$ intervals within the 7 drill sites we investigated: PPLC-5 (4737-4465 ka), PPLC-4 (3 intervals between 4093 and 2915 ka), PPLC-3 (2 intervals on either side of a CaCO3 high, between 2684 and 2248 ka), PPLC-2 (2135-1685 ka), and PPLC-1 (402-51 ka). We found that PPLC-5 and PPLC-2 result from $CaCO_3$ dilution through diatom production, and the other 3 result from enhanced $CaCO_3$ dissolution.

The magnitude of $CaCO_3$ dissolution can be described by changes in the CCD. However, local and regional variability of sedimentation restricts information that can be extracted from the CCD approach to large changes and/or low time resolution. The ratio $CaCO_3$:$BaSO_4$ makes it possible to study dissolution at an individual drill site. We used this ratio to show that 100-kyr dissolution cycles were regionally strong by 1600 ka, in contrast to oxygen isotopes which didn't develop 100-kyr cyclicity until about 1000 ka. We also used $CaCO_3$:$BaSO_4$ to confirm that the highest $CaCO_3$ dissolution occurred in PPLC-4, whose 3 sub events occurred between 4 and 3 Ma.

It is possible that PPLC-4 resulted from closure of the CAS, but there are complicating factors, like the abrupt shift of the locus of $CaCO_3$ burial eastward in the Pacific at the end of PPLC-5, the last high deposition interval of the LMBB. High flushing of the Atlantic basin is indicated by the Atlantic-Pacific $\delta^{13}C$ gradient, but the gradient was actually weakening in the 4-3 Ma interval suggesting more Antarctic DIC storage or more total DIC in the ocean. New work concludes that atmospheric CO_2 was declining in this interval (Stap et al, 2016) and is also associated with declining but still high global SST (Herbert et al, 2016), and these changes need to be factored in as well.

Acknowledgments

We thank all the members of IODP Expedition 320/321 and those from ODP Leg 138 (Scientists, technicians, drillers, and ships crew) who collected the basic information and sediments needed for this study. Lyle was funded by NSF grant OCE-0962184 and grant OCE-1656960. Westerhold and Drury were funded by the Deutsche Forschungsgemeinschaft (DFG) grant WE5479-1 and WE5479-3. Jun Tian was funded by National Science Foundation of China (Grant No. 41525020, 41776051) and Program of Shanghai Subject Chief Scientist (A type) (16XD1403000).

References

Balakrishnan Nair, T. M., Ittekkot, V., Shankar, R. and Guptha, M. V. S.: Settling barium fluxes in the Arabian Sea: Critical evaluation of relationship with export production, Deep Sea Research II, 52, 1930-1946, doi:10.1016/j.dsr2.2005.06.00, 2005.

Barron, J., Lyle, M. and Koizumi, I.: Late Miocene and early Pliocene biosiliceous sedimentation along the California margin, Revista Mexicana de Ciencias Geologicas, 19, 161-169, 2002.

Bell, D. B., Jung, S. J. A., Kroon, D., Hodell, D. A., Lourens, L. J. and Raymo, M. E.: Atlantic deep-water response to the early Pliocene shoaling of the Central American Seaway, Scientific Reports, 5, 12552, doi:10.1038/srep12252, 2015.

Berger, W. H.: Biogenous deep-sea sediments: fractionation by deep-sea circulation, Geological Society of America Bulletin, 81, 1385-1402, 1970.

Berger, W. H.: Cenozoic sedimentation in the eastern tropical Pacific, Geological Society of America Bulletin, 84, 1941-1954, 1973.

Bloomer, S. F., and Mayer, L. A.: Core-log-seismic integration as a framework for determining the basin-wide significance of regional reflectors in the eastern equatorial Pacific, Geophysical Research Letters, 24, 321-334, 1997.

Boudreau, B. P., Middelburg, J. J., and Meysman, F. J. R.: Carbonate compensation dynamics, Geophysical Research Letters, 37, L03603, doi:10.1029/2009GL041847, 2010.

Chuey, J. M., Rea, D. K., and Pisias, N. G.: Late Pleistocene paleoclimatology of the central equatorial Pacific: a quantitative record of eolian and carbonate deposition, Quaternary Research, 28, 323-339, 1987.

Coxall, H. K., Wilson, P. A., Pälike, H., Lear C. and Backman, J.: Rapid stepwise onset of Antarctic glaciation and deeper calcite compensation in the Pacific Ocean, Nature, 433, 53-57, 2005.

Dickens, G. R. and Barron, J. A.: A rapidly deposited pennate diatom ooze in upper Miocene-lower Pliocen sediment beneath the North Pacific polar front, Marine Micropaleontology, 31, 177-182, 1997.

Dickens, G. R. and Owen, R. M.: The latest Miocene-early Pliocene biogenic bloom: a revised Indian Ocean perspective, Marine Geology, 161, 75-91, 1999.

Diester-Haass, L., Meyers, P. A. and Vidal, L.: The late Miocene onset of high productivity in the Benguela Current upwelling system as part of a global pattern, Marine Geology, 180, 87-103, 2002.

Drury, A. J., John, C. M., and Shevenell, A. E.: Evaluating climatic response to external radiative forcing during the late Miocene to early Pliocene: New perspectives from eastern equatorial Pacific (IODP U1338) and North Atlantic (ODP982) locations, Paleoceanography, 31, 167-184, doi:10.1002/2015PA002881, 2016.

Drury, A. J., Westerhold, T., Frederichs, T., Tian, J., Wilkens, R., Channell, J. E. T., Evans, H., John, C. M., Lyle, M., and Röhl, U.: Late Miocene climate and time scale reconciliation: Accurate orbital calibration from a deep-sea perspective, Earth and Planetary Science Letters, 475, 254-266, doi:10.1016/j.epsl.2017.07.038, 2017.

Drury, A. J., Lee, G. P., Gray, W. R., Lyle, M., Westerhold, T., Shevenell, A. E., and John, C. M.,: Deciphering the state of the late Miocene to early Pliocene equatorial Pacific, Paleoceanography and Paleoclimatology, 33, 246-263, doi:10.1002/2017PA003245, 2018.

Dymond, J., Suess, E. and Lyle, M.: Barium in deep-sea sediment: A geochemical proxy for paleoproductivity, Paleoceanography, 7, 163-181, 1992.

Dymond, J., and Collier, R.: Particulate barium fluxes and their relationships to biological productivity, Deep Sea Research II, 43, 1283-1308, 1996.

Farrell, J. W., and Prell, W. L.: Climatic change and $CaCO_3$ preservation: an 800,000 year bathymetric reconstruction from the central equatorial Pacific Ocean, Paleoceanography, 4, 447-466, 1989.

Farrell, J. W., and Prell, W. L.: Pacific $CaCO_3$ preservation and $\delta^{18}O$ since 4 Ma: Paleoceanic and paleoclimatic implicatons, Paleoceanography, 6, 485-499, 1991.

Farrell, J. W., Raffi, I., Janecek, T. R., Murray, D. W., Levitan, M., Dadey, K. A., Emeis, K.-C., Lyle, M., Flores, J.-A. and Hovan, S.: Late Neogene sedimentation patterns in the eastern equatorial Pacific Ocean. In: Proceedings of the Ocean Drilling Program, Scientific Results, 138, 717-756, 1995.

Filipelli, G. M.: Intensification of the Asian monsoon and a chemical weathering event in the late Miocene-early Pliocene: Implications for late Neogene climate change, Geology, 25, 27-30, doi:10.1130/0091-7613,1997.

Francois, R., Frank, M., Rutgers van der Loeff, M. M. and Bacon, M. P.: ^{230}Th-normalization: an essential tool for

interpreting sedimentary fluxes during the late Quaternary, Paleoceanography, 19, doi:10.1029/2003PA000939, 2004.

Grant, K. M., and Dickens, G. R.: Coupled productivity and carbon isotope records in the southwest Pacific Ocean during the late Miocene-early Pliocene biogenic bloom, Palaeogeography, Palaeoclimatology, Palaeoecology, *187*, 61-82, 2002.

Griffith, E. M. and Paytan, A.: Barite in the ocean--occurence, geochemistry and palaeoceanographic applications, Sedimentology, 59, 1817-1835, doi:10.1111/j.1365-3091.2012.01327, 2012.

Hagelberg, T. K., Pisias, N. G., Mayer, L. A., Shackleton, N. J., and Mix, A. C.: Spatial and temporal variability of late Neogene equatorial Pacific Carbonate: Leg 138. . In: Proceedings of the Ocean Drilling Program, Scientific Results, 138, 321-336, 1995.

Harris, S. E., Mix, A. C. and King, T.: Biogenic and terrigenous sedimentation at Ceara Rise, western tropical Atlantic, supports Pliocene-Pleistocene Deep-water linkage between hemispheres, in *Proceedings of the Ocean Drilling Program, Scientific Results*, 154, 331-345, 1997.

Hays, J. D., Saito, T., Opdyke, N. D., and Burckle, L. H.: Pliocene-Pleistocene sediments of the equatorial Pacific: Their paleomagnetic, biostratigraphic, and climatic record, Geological Society of America Bulletin, 80, 1481-1514, 1969.

Herbert, T. D., Lawrence, K. T., Tzanova, A., Peterson, L. C., Caballero-Gill, R. and Kelly, C. S.: Late Miocene global cooling and the rise of modern ecosystems., Nature Geoscience, 9, 843-847, doi:10.1038/NGEO2813, 2016.

Hodell, D. A., Charles, C. D. and Sierro, F. J.: Late Pleistocene evolution of the ocean's carbonate system, Earth and Planetary Science Letters, 192, 109-124, 2001.

Holbourn, A., Kuhnt, W., Lyle, M., Schneider, L., Romero, O., and Andersen, N.: Middle Miocene climate cooling linked to intensification of eastern equatorial Pacific upwelling, Geology, 42, 19-22, doi:10.1130/G34890.1, 2014.

Honjo, S., Dymond, J., Collier, R., and Manganini, S. J.: Export production of particles to the interior of the equatorial Pacific Ocean during the 1992 EqPac experiment, Deep-Sea Research II, 42, 831-870, 1995.

Kemp, A. E. S. and Baldauf, J. G.: Vast Neogene laminated diatom mat deposits from the eastern equatorial Pacific Ocean, Nature, 362, 141-144, 1993.

Kleiven, H. F., Jansen, E., Curry, W. B., Hodell, D. A. and Venz, K.:, Atlantic Ocean thermohaline circulation changes on orbital to suborbital timescales during the mid-Pleistocene, *Paleoceanography*, *18*, 1, doi:10.1029/2001PA000629, 2003.

Klevenz, V., Vance, D., Schmidt, D. N. and Mezger, K.:Neodymium isotopes in benthic foraminifera: Core-top systematics and a down-core record from the Neogene south Atlantic, *Earth and Planetary Science Letters*, *265*, 571-587, doi:10.1016/j.epsl.2007.10.053, 2008.

Lawrence, K. T., Liu, Z. and Herbert, T. D.: Evolution of the eastern tropical Pacific through Plio-Pleistocene glaciation, Science, 312, 79-83, doi:10.1126/science.1120395, 2006.

Liao, Y. and Lyle, M.: Late Miocene to Pleistocene sedimentation and sediment transport on the Cocos Ridge, eastern tropical Pacific Ocean, Marine Geology, 355, 1-14, doi:10.1016/j.margeo.2014.05.007, 2014.

Lisiecki, L. E. and Raymo, M. E.: A Pliocene-Pleistocene stack of 57 globally distributed benthic $\delta^{18}O$ records, Paleoceanography, 20, PA1003, doi:10.1029/2004PA001071, 2005.

Lyle, M., Mitchell, N. C., Pisias, N., Mix, A., Martinez, J. I. and Paytan, A.: Do geochemical estimates of sediment focusing pass the sediment test in the equatorial Pacific, Paleoceanography, 20, doi:10.1029/2004PA001019, 2005a.

Lyle, M. W.,Olivarez Lyle, A., Backman, J. and Tripati, A.: Biogenic sedimentation in the Eocene equatorial Pacific: the stuttering greenhouse and Eocene carbonate compensation depth. In: Proceedings of the Ocean Drilling Program, Scientific Results, Leg 199, 1-35, doi:10.2973/odp.proc.sr.199.219.2005, 2005b.

Lyle, M., Olivarez Lyle, A., Gorgas, T., Holbourn, A., Westerhold, T., Hathorne, E. C., Kimoto, K. and Yamamoto, S.: Data report: raw and normalized elemental data along the U1338 splice from X-ray Fluorescence scanning, Proceedings of the Integrated Ocean Drilling Program, 320/321,doi: 10.2204/iodp.proc.320321.2010, 2012.

Lyle, M. and Backman, J.: Data Report: Calibration of XRF-estimated $CaCO_3$ along the Site U1338 splice, Proceedings of the Integrated Ocean Drilling Program, 320/321, doi: 10.2204/iodp.proc.320321.205.2013, 2013.

Lyle, M., Marcantonio, F., Moore, W. S., Murray, R. W., Huh, C.-A., Finney, B. P., Murray, D. W. and Mix, A. C.: Sediment size fractionation and sediment focusing in the equatorial Pacific: effect on ^{230}Th normalization and paleoflux measurements, Paleoceanography, 29, 747-763, doi:10.1002/2014PA002616, 2014.

Lyle, M., and Baldauf, J.: Biogenic sediment regimes in the Neogene equatorial Pacific, IODP Site U1338: Burial, production, and diatom community, Palaeogeography, Palaeoclimatology, Palaeoecology, 433, 106-128, doi:10.1016/j.palaeo.2015.04.001, 2015.

Marcantonio, F., Lyle, M. and Ibrahim, R.: Particle sorting during sediment redistribution processes and the effect on ^{230}Th-normalized mass accumulation rates, Geophysical Research Letters, 41, 5547-5554, doi:10.1002/2014GL060477, 2014.

Mayer, L. A., Shipley, T. H., and Winterer, E. L.: Equatorial Pacific seismic reflectors as indicators of global oceanographic events, Science, 233, 761-764, 1986.

Mayer, L. A.: Extraction of high-resolution carbonate data for palaeoclimate reconstruction, Nature, 352, 148-150, 1991.

Mayer, L. A., Pisias, N. G., Janecek, T., and Leg_138_Shipboard_Scientific_Party: Proceedings of the Ocean Drilling Program, Initial Reports, 138, Ocean Drilling Program, College Station TX, 1992.

Miller, K. G., Kominz, M. A., Browning, J. V., Wright, J. D., Mountain, G. S., Katz, M. E., Sugarman, P. J., Cramer, B. S., Christie-Blick, N. and Pekar, S. F.: The Phanerozoic record of global sea-level change, Science, 310, 1293-1298, doi:10.1126/science.1116412, 2005.

Milliman, J. D., and Droxler, A. W.: Neritic and pelagic carbonate sedimentation in the marine environment: ignorance is not bliss, Geologische Rundschau, 85, 496-504, 1996.

Mitchell, N. C. and Huthnance, J. M.: Geomorphological and geochemical evidence (^{230}Th anomalies) for cross-equatorial currents in the central Pacific, Deep Sea Research I, 178, 24-14, doi: 10.1016/j.dsr.2013.04.003 , 2013.

Mix, A. C., Pisias, N. G., Rugh, W., Wilson, J., Morey, A., and Hagelberg, T. K.: Benthic foraminifer stable isotope record from Site 849 (0-5 Ma): local and global climate change. . In: Proceedings of the Ocean Drilling Program, Scientific Results, 138, 371-412, 1995.

Molnar, P., England, P., and Martinod, J.: Mantle dynamics, uplift of the Tibetan Plateau, and the Indian monsoon, Reviews of Geophysics, 31, 357-396, 1993.

Molnar, P.: Closing of the Central American Seaway and the Ice Age: A critical review, Paleoceanography, 23, doi: 10.1029/2007PA001574, 2008.

Molnar, P.: Comment (2) on "Formation of the Isthmus of Panama" by O'Dea et al, Science Advances, 3, doi: 10.1126/sciadv.1602320, 2017.

Murray, R. W., Knowlton, C., Leinen, M., Mix, A. and Polsky, C. H.: Export production and carbonate dissolution in the central equatorial Pacific Ocean over the past 1 Myr, Paleoceanography, 15, 570-592, 2000.

NASA Goddard Space Flight Center, Ocean Ecology Laboratory, Ocean Biology Processing Group. Sea-viewing Wide Field-of-view Sensor (SeaWiFS) Particulate Organic Carbon Data; 2014 Reprocessing. NASA OB.DAAC, Greenbelt, MD, USA. doi: 10.5067/ORBVIEW-2/SEAWIFS/L3B/POC/2014.Accessed on 01/26/2018

O'Dea, A. Lessios, H. A., Coates, A. G., Eytan, R. I., Restrepo-Moreno, S. A., Cione, A. L., Collins, L. S., de Queiroz, A., Farris, D. W., Norris, R. D., Stallard, R. F., Woodbourne, M. O., Aguilera, O., Aubry, M.-P., Berggren, W. A., Budd, A. F., Cossuol, M. A., Coppard, S. E., Duque-Caro, H., Finnegan, S., Gasparini, G. M., Grossman, E. L., Johnson, K. G., Keigwin, L. D., Knowlton, N., Leigh, E. G., Leonard-Pingel, J. S., Marko, P. B., Pyenson, N. D., Rachello-Dolmen, P., Soibelzon, E., Soibelzon, L., Todd, J. A., Vermeiz, G. J. and Jackson, J. B. C.: Formation of the Isthmus of Panama, Science Advances, 2, doi:10.1126/sciadv.1600883, 2016.

ODP Leg 202 Shipboard Scientific Party. Leg 202 summary. *Proc. ODP, Init. Repts.,* 202: College Station, TX (Ocean Drilling Program), 1–145. doi:10.2973/odp.proc.ir.202.101.2003, 2003.

Opdyke, B. N. and Wilkinson, B. H.: Surface area control of shallow cratonic to deep marine carbonate accumulation, Paleoceanography, 3, 685-703, 1988.

Pälike, H., Lyle, M., Nishi, H., Raffi, I., Gamage, K., Klaus, A., and the Expedition 320/321 Scientists, *Proc. IODP*, 320/321: Tokyo (Integrated Ocean Drilling Program Management International, Inc.). doi:10.2204/iodp.proc.320321.2010, 2010b.

Pälike, H., Nishi, H., Lyle, M., Raffi, I., Gamage, K., Klaus, A., and the Expedition 320/321 Scientists. Expedition 320/321 summary, *Proc. IODP*, 320/321, doi:10.2204/iodp.proc.320321.101.2010, 2010b.

Pälike, H., Lyle, M., Nishi, H., Raffi, I., Ridgwell, A., Gamage, K., Klaus, A., Acton, G. D., Anderson, L., Backman, J., Baldauf, J., Beltran, C., Bohaty, S. M., Bown, P., Busch, W., Channell, J. E. T., Chun, C. O. J., Delaney, M., Dewangan, P., Dunkley Jones, T., Edgar, K. M., Evans, H., Fitch, P., Foster, G. L., Gussone, N., Hasegawa, H.,

Hathorne, E. C., Hayashi, H., Herrle, J. O., Holbourn, A., Hovan, S., Hyeong, K., Iijima, K., Ito, T., Kamikuri, S., Kimoto, K., Kuroda, J., Leon-Rodrigues, L., Malinverno, A., Moore, T. C. jr., Murphy, B. H., Murphy, D. P., Nakamura, H., Ogane, K., Ohneiser, C., Richter, C., Robinson, R., Rohling, E. J., Romero, O., Sawada, K., Scher, H., Schneider, L., Sluijs, A., Takata, H., Tian, J., Tsujimoto, A., Wade, B. S., Westerhold, T., Wilkens, R., Williams, T., Wilson, P. A., Yamamoto, Y., Yamamoto, S., Yamazaki, T., and Zeebe, R.: A Cenozoic record of the equatorial Pacific carbonate compensation depth, Nature, 488, 609-614, doi:10.1038/nature11360, 2012.

Peterson, L. C., Murray, D. W., Ehrmann, W. U., and Hempel, P.: Cenozoic carbonate accumulation and compensation depth changes in the Indian Ocean. In: Synthesis of Results from Scientific Drilling in the Indian Ocean, R. A. Duncan, D. K. Rea, R. B. Kidd, U. von Rad and J. K. Weissel (Eds.), Geophysical Monograph, 70, American Geophysical Union, Washington D.C., 311-331,1992.

Poore, H. R., Samworth, R., White, N. J., Jones, S. M. and McCave, I. N.: Neogene overflow of Northern Component Water at the Greenland-Scotia Ridge, Geochemistry, Geophysics, Geosystems, 7, Q06010, doi:10.1029/2005GC001085, 2006.

Povea, P., Cacho, I., Moreno, A., Pena, L. D., Menendez, M., Calvo, E., Canals, M., Robinson, R. S., Mendez, F. J. and Flores, J.-A.: Atmosphere-ocean linkages in the eastern equatorial Pacific over the early Pleistocene, Paleoceanography, 31, doi:10.1002/2015PA002883, 2016.

Rohling, E. J., Foster, G. L., Grant, K. M., Marino, G., Roberts, A. P., Tamisiea, M. E. and Williams, F.: Sea-level and deep-sea-temperature variability over the past 5.3 million years, Nature, 508, 477-482, doi: 10.1038/nature13230, 2014.

Roth, J. M., Droxler, A. W. and Kameo, K.: The Caribbean carbonate crash at the middle to late Miocene transition: linkage to the establishment of the modern global ocean conveyer, Proceedings of the Ocean Drilling Program, Scientific Results, 165, 249-273, doi:10.2973/odp.proc.sr.165.013.2000, 2000.

Ruddiman, W. F., Raymo, M. E., Martinson, D. G., Clement, B. M., and Backman, J.:, Pleistocene evolution: Northern hemisphere ice sheets and North Atlantic Ocean, *Paleoceanography*, *4*,4, 353-412, 1989

Seki, O., Foster, G. L., Schmidt, D. N., Mackenson, A., Kawamura, K. and Pancost, R. D.: Alkenone and boron-based Pliocene pCO2 records, Earth and Planetary Science Letters, 292, 201-211, doi:10.1016/j.epsl.2010.01.037, 2010.

Seki, O., Schmidt, D. N., Schouten, S., Hopmans, E. C., Sininghe Damste, J. S. and Pancost, R. D. : Paleoceanographic changes in the eastern equatorial Pacific over the last 10 Myr, *Paleoceanography*, *27*, PA3224, doi:10.1029/2011PA002158, 2012.

Shackford, J. K., Lyle, M., Wilkens, R., and Tian, J.: Data report: raw and normalized elemental data along the Site U1335, U1336, and U1337 splices from X-ray fluorescence scanning Proceedings of the Integrated Ocean Drilling Program, 320/321, doi:10.2204/iodp.proc.320321.216.2014, 2014.

Stap, L. B., de Boer, B., Ziegler, M., Bintanja, R. and Lourens, L. J.: CO_2 over the past 5 million years: continuous simulation and new d11B-based proxy data, Earth and Planetary Science Letters, 439, 1-10, doi:10.1016/j.epsl.2016.01.022, 2016.

Tian, J., Ma, X., Zhou, J., Jiang, X., Lyle, M., Shackford, J. K., and Wilkens, R. : Paleoceanography of the east equatorial Pacific over the past 16 Myr and Pacific-Atlantic comparison: High resolution benthic foraminiferal $\delta^{18}O$ and $\delta^{13}C$ records at IODP Site U1337, *Earth and Planetary Science Letters*, *499*, 185-196, doi:10.1016/j.epsl.2018.07.025, 2018.

Tominaga, M. Lyle, M. and Mitchell, N. C.: Seismic interpretation of pelagic sedimentation regimes in the 18–53 Ma eastern equatorial Pacific: Basin-scale sedimentation and infilling of abyssal valleys, Geochemistry, Geophysics, Geosystems, 12, Q03004, doi:10.1029/2010GC003347, 2011.

van Andel, Tj. H. and Moore, T. C. jr.: Cenozoic calcium carbonate distribution and calcite compensation depth in the central equatorial Pacific Ocean, Geology, 2, 87-92, 1974.

van Andel, Tj. H., Heath, G. R., and Moore, T. C. jr.: Cenozoic History and Paleoceanography of the central equatorial Pacific Ocean, GSA Memoir 143, Geological Society of America, 1975.

Wilkens, R., Westerhold, T., Drury, A. J., Lyle, M., Gorgas, T. and Tian, J.: Revisiting the Ceara Rise, equatorial Atlantic Ocean: isotope stratigraphy of ODP Leg 154 from 0 to 5 Ma, Climate of the Past, 13, 779-793, doi:10.5194/cp-13-779-2017, 2017.

Wilson, J. K.: Early Miocene carbonate dissolution in the eastern equatorial Pacific, Phd thesis, Oceanography, Texas A and M University, 155 pp., 2014.

Winckler, G., Anderson, R. F., Fleisher, M. Q., McGee, D., and Mahowald, N.: Covariant Glacial-Interglacial dust fluxes in the equatorial Pacific and Antarctica, Science, 320, 93-96, doi:10.1126/science.1150595, 2008.

Zeebe, R., and Caldeira, K.: Close mass balance of long-term carbon fluxes from ice-core CO_2 and ocean chemistry records, Nature Geoscience, 1, 312-315, doi:10.1038/ngeo185, 2008.

Ziegler, C. L., Murray, R. W., Plank, T. and Hemming, S. R.: Sources of Fe to the equatorial Pacific Ocean from the Holocene to Miocene, Earth and Planetary Science Letters, 270, 258-270, doi:10.1016/j.epsl.2008.03.044, 2008.

Clim. Past Discuss., https://doi.org/10.5194/cp-2018-157
Manuscript under review for journal Clim. Past
Discussion started: 7 December 2018

Climate of the Past Discussions
Open Access
EGU

Table 1: Drill Sites in this study

Site	Latitude (°N)	Longitude(°E)	Water depth (mbsl)	Length (ka) of dated record	5 Ma Latitude(°N)	5 Ma longitude (°E)	Data Available
848	-2.994	-110.480	3854	8180	-3.77	-106.09	GRA-CaCO3
849	0.183	-110.520	3838	7204	-0.60	-106.25	scanning XRF, GRA CaCO3
850	1.297	-110.521	3786	8172	0.51	-106.30	GRA-CaCO3
851	2.770	-110.572	3760	8180	1.98	-106.41	GRA-CaCO3
U1338	2.508	-117.970	4206	8180	1.43	-113.79	scanning XRF
U1337	3.834	-123.206	4468	8180	2.55	-119.07	scanning XRF
U1335	5.312	-126.284	4333	8180	3.92	-122.19	scanning XRF

Table 2 Plio-Pleistocene Low Carbonate Intervals (PPLCs)

Low carbonate interval	Age Interval(ka)	Interval length kyr	MIS at Site 849	Magnetic Chron	Depth Site U1338 (m CCSF)	Depth Site 849 (m CCSF)	Depth Site 848 (m CCSF)	Depth Site 850 (m CCSF)	Depth Site 851 (m CCSF)	Depth Site U1337 (m CCSF)	Depth Site U1335 (m CCSF)
PPLC-01	51-402	351	4-11	C1n	1.06-5.14	1.71-12.71	0.81-5.53	1.17-8.52	0.78-4.07	0.79-5.87	0.55-2.68
PPLC-02	1685-2135	450	59-81	lower C1r.2r to base C2r.1r	22.20-28.77	48.77-61.38	25.02-27.70	34.98-42.71	31.93-39.64	25.21-31.73	10.13-12.10
PPLC-03a	2248-2383	193	87-93	C2r	29.23-31.56	62.61-67.23	28.15-29.68	43.81-47.91	39.92-42.11	32.27-34.81	12.27-13.32
PPLC-03b	2532-2684	152	100-G1	C2r/C2An.1n	33.59-35.71	71.10-74.94	30.84-31.61	51.13-54.70	45.17-47.34	36.50-39.30	14.12-14.98
PPLC-04a	2915-3372	457	G16-MG4	lower C2An.1n to upper C2An.3n	39.19-45.84	81.14-93.52	33.20-35.37	60.44-69.81	52.91-61.06	43.07-51.79	16.33-18.39
PPLC-04b	3558-3731	173	MG12-Gi 11	lower C2An.3n to upper C2Ar	48.24-50.85	97.68-102.36	35.83-37.12	73.45-77.31	64.46-66.95	54.34-57.93	19.04-19.68
PPLC-04c	3834-4093	258	Gi 16-Gi 24	lower C2Ar	52.42-56.35	105.69-112.51	37.54-38.68	80.02-85.25	68.95-72.75	60.45-67.45	20.06-21.18
PPLC-05	4465-4737	272	N2-NS 6	base C3n.1r to lower C3n.2r	62.69-69.33	123.91-143.00	40.35-44.27	94.10-107.72	80.42-87.55	missing	missing

Clim. Past Discuss., https://doi.org/10.5194/cp-2018-157
Manuscript under review for journal Clim. Past
Discussion started: 7 December 2018

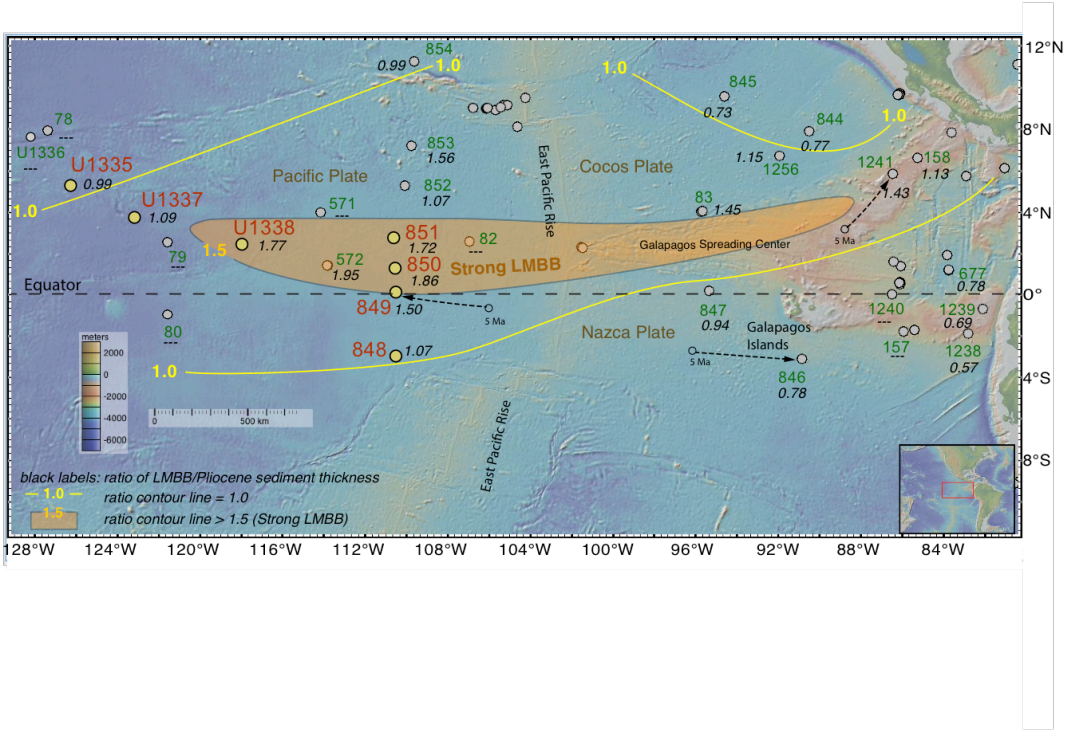

Figure 1: Red site labels: ODP and IODP drill sites from the eastern equatorial Pacific used in this paper with other DSDP/ODP/IODP Sites labeled in green. All sites are at their modern locations. Example backtracked positions at 5 Ma are shown for Site 849 on the Pacific Plate (representative for U1335, U1337, U1338, and Sites 848-854), Site 846 on the Nazca Plate (representative for Sites 847, 1238, and 1239), and Site 1241 on the Cocos Plate (representative for Sites 844, 845, and 1256), assuming a hotspot reference frame. Sites U1335, U1337, U1338, and 849 have XRF scanning chemical data, while Sites 848,850, and 851 have $CaCO_3$% estimated from bulk density. Thickness of the 8.5-4.5 Ma sediment divided by the 4.5-0 Ma sediment thickness (LMBB/Pliocene ratio) are indicated by the italic black labels at each drill site. Sites on crust younger than 8 Ma, or where the section was incompletely drilled, or with a hiatus in the interval are marked with "---". Yellow lines mark where the LMBB/Pliocene ratio is 1, while shaded orange region is where the ration is >1.5, marking the major LMBB locus of deposition. Thickest LMBB sequences are found on sites with crust older than 8 Ma on the Pacific and Cocos Plates just north of the equator. Sites south of the equator in the easternmost Pacific have thicker sediments in the 4.5-0 Ma time range, indicating high young sedimentation rates.

Clim. Past Discuss., https://doi.org/10.5194/cp-2018-157
Manuscript under review for journal Clim. Past
Discussion started: 7 December 2018

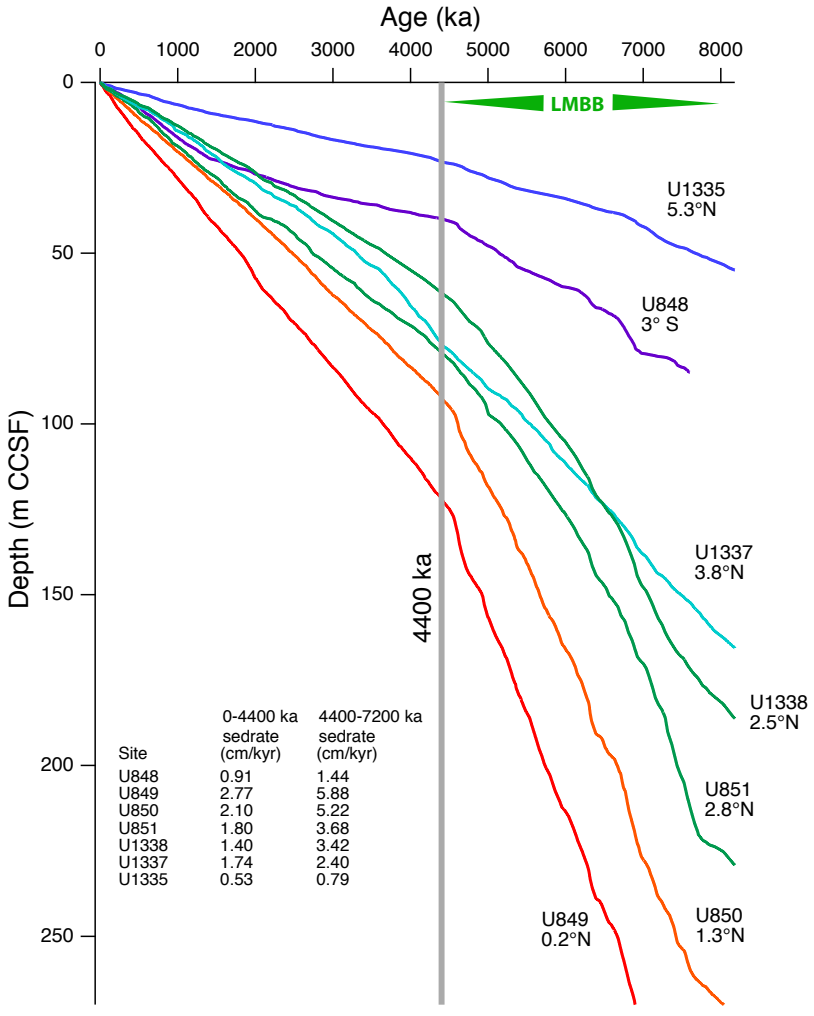

Figure 2: Age-depth curves for ODP Leg 138 Sites 848,849,850, and 851 with IODP Exp 320/321 Sites U1335, U1337, and U1338, based on age model in this paper. Steeper slopes represent faster sedimentation rates. Steepest slopes are found at sites that are nearest to the high productivity equatorial upwelling zone. Average sedimentation rates for the section younger than 4400 ka and for rates between 7200 ka (base of XRF section scanned in Site 849) and 4400 ka are tabulated. The break in sedimentation at about 4400 ka marks the end of the late Miocene Biogenic Bloom LMBB). CCSF (Composite Coring depth below Sea Floor) is the depth within the continuous spliced sediment section

Clim. Past Discuss., https://doi.org/10.5194/cp-2018-157
Manuscript under review for journal Clim. Past
Discussion started: 7 December 2018

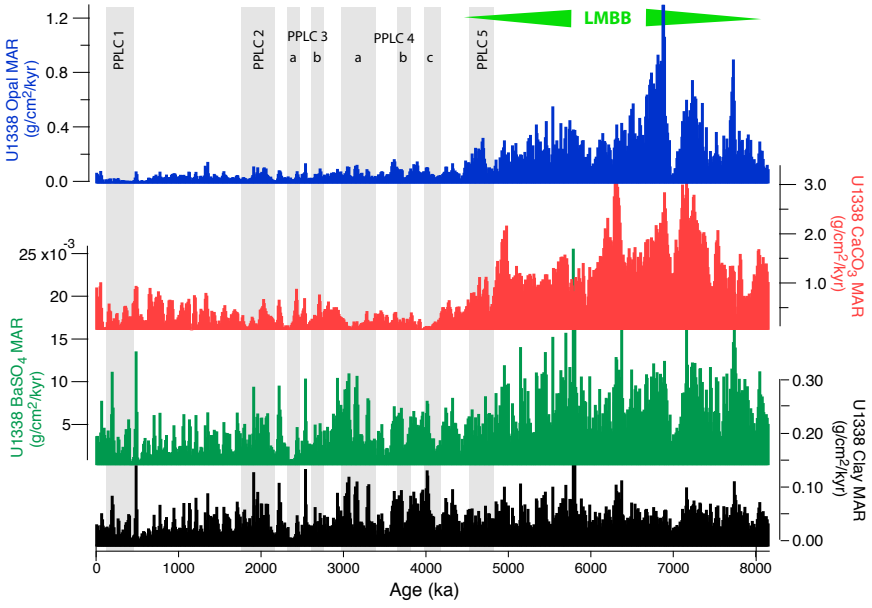

Figure 3: Mass Accumulation Rates (MAR) of biogenic sediment components and clay at Site U1338 to show the improved MAR resolution in this paper (10 kyr) versus Lyle and Baldauf (2015, 200 kyr intervals 5 Ma, 500 kyr intervals from 5-16 Ma). Gray bands mark PPLCs (Pliocene-Pleistocene Low $CaCO_3$ intervals). High opal and $CaCO_3$ MAR prior to 4465 ka represents the LMBB interval at Site U1338. Clay MAR is relatively constant over the 8 million years shown.

Clim. Past Discuss., https://doi.org/10.5194/cp-2018-157
Manuscript under review for journal Clim. Past
Discussion started: 7 December 2018

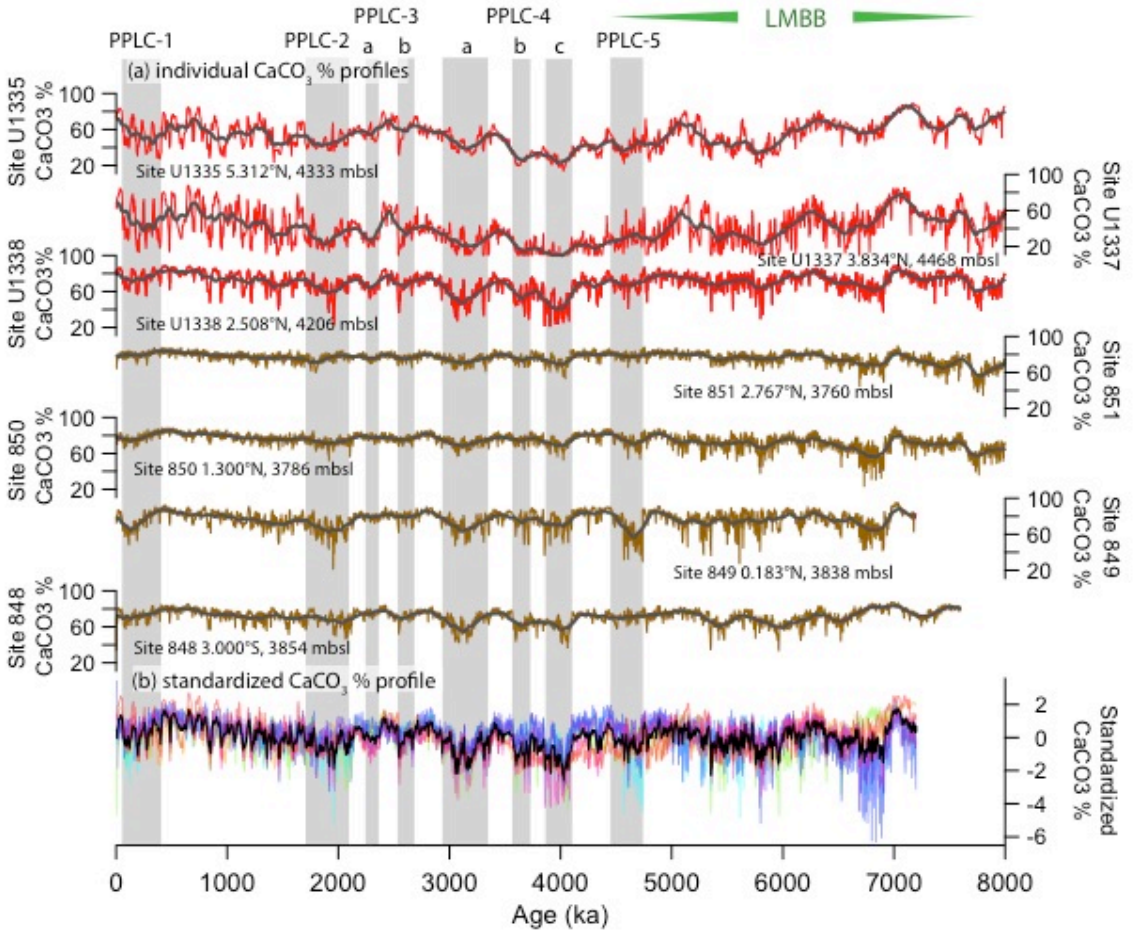

Figure 4: (a) $CaCO_3$ wt % profiles from the 7 drill sites in this paper. Red profiles are from sites drilled by IODP Exp 320/321 while the brown profiles are sites drilled on ODP Leg 138. The gray shading marks PPLC intervals determined in this paper (See Table 2). LMBB is the Late Miocene Biogenic Bloom and includes PPLC-5, actually early Pliocene in age. (b) Stacked and standardized $CaCO_3$ % profiles. Each profile is expressed in standard deviations from the mean and are represented by the colored profiles. The black profile is the stack of all the $CaCO_3$ % curves. The PPLCs were determined by common low $CaCO_3$ % in the profiles.

Clim. Past Discuss., https://doi.org/10.5194/cp-2018-157
Manuscript under review for journal Clim. Past
Discussion started: 7 December 2018

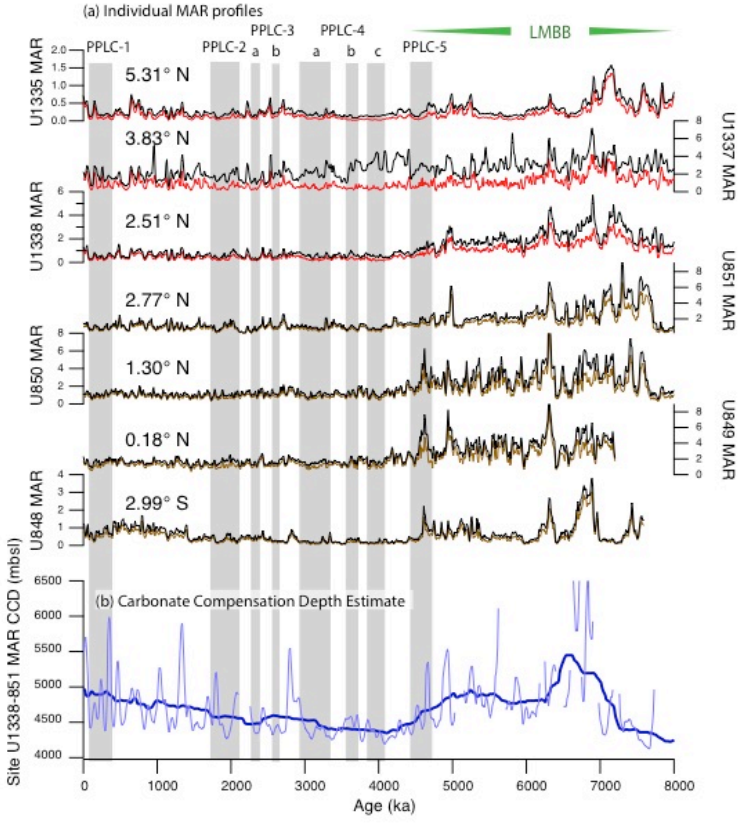

Figure 5: (a) Mass Accumulation Rates (MARs) for eastern equatorial Pacific drill sites. Bulk MAR (black) and $CaCO_3$ MAR (brown—Leg 138; red—Exp 320/ I21) profiles from drill sites studied for this paper. MAR data are at 10 kyr intervals. Sites are arranged from south to north, at their modern position. Only Site U1337 has bulk MAR time series that diverge significantly from the $CaCO_3$ MAR profiles, indicative of sediment focusing at Site U1337. (b) Eastern Pacific CCD change using the gradient of deposition from Site 851 (3760 m) to Site U1338 (4206 m) with two levels of smoothing, 50 kyr and 750 kyr. Breaks in the record are intervals where the CaCO3 MAR at Site U1338 exceeded that at Site 851. The 50-kyr smooth finds transient CCD changes up to 1.5 km. The 750-kyr smooth displays how the CCD was shallowest between 4200 and 3100 ka, during the time of PPLC-4.

Clim. Past Discuss., https://doi.org/10.5194/cp-2018-157
Manuscript under review for journal Clim. Past
Discussion started: 7 December 2018

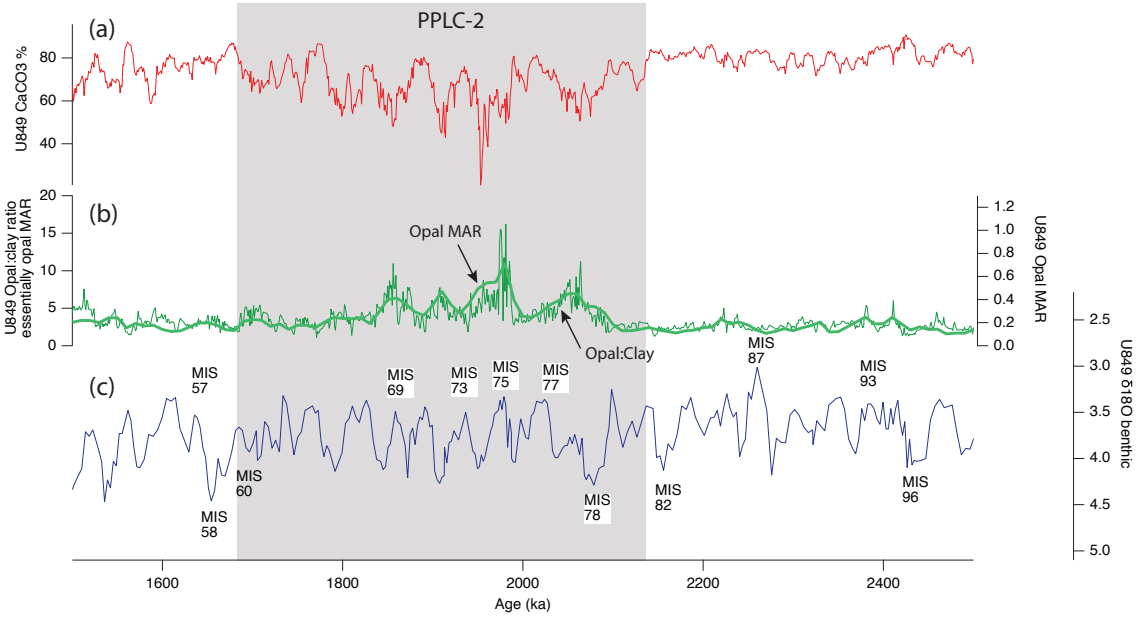

Figure 6: Site 849 profiles over low carbonate interval PPLC-2 (2135-1685 ka) showing opal dilution as a primary cause of the low $CaCO_3$ %. (a) $CaCO_3$% estimated by scanning XRF; (b) Thick line is Opal MAR, and thin line is opal:clay ratio, showing the high opal MAR associated with each sub-interval in PPLC-2. (c) Benthic oxygen isotope stratigraphy constructed with data from Mix et al. (1995). Stages are numbered following Lisiecki and Raymo (2005).

Clim. Past Discuss., https://doi.org/10.5194/cp-2018-157
Manuscript under review for journal Clim. Past
Discussion started: 7 December 2018

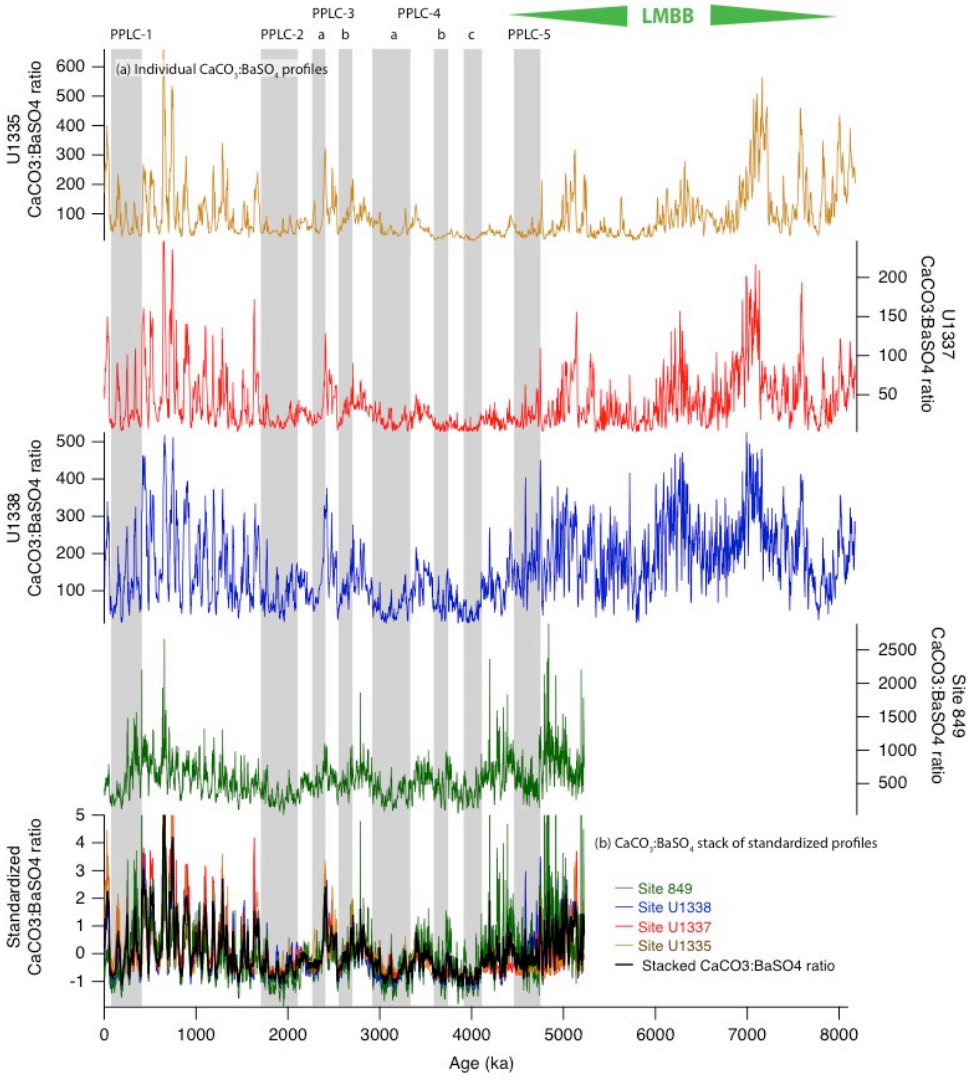

Figure 7: XRF $CaCO_3$:$BaSO_4$ profiles to investigate $CaCO_3$ dissolution at drill sites with scanning XRF profiles, assuming high and consistent preservation in sediments of $BaSO_4$ fixed by organic matter production, and relatively stable ratios of $CaCO_3$:$BaSO_4$ in the particulate rain (Lyle and Baldauf, 2015). Low $CaCO_3$:$BaSO_4$ indicates high dissolution of $CaCO_3$. (a) Individual profiles of $CaCO_3$:$BaSO_4$ at Sites U1335, U1337, U1338 and Site 849. Note how ratios are higher at Site 849, at the equator and shallow with respect to the other sites. (b) Changes in dissolution in the eastern Pacific shown by stacked $CaCO_3$:$BaSO_4$ records atandardized to standard deviations from the average. Low $CaCO_3$:$BaSO_4$ coincides with PPLC's, indicating that the dissolution signal has an important impact on the record.

Clim. Past Discuss., https://doi.org/10.5194/cp-2018-157
Manuscript under review for journal Clim. Past
Discussion started: 7 December 2018

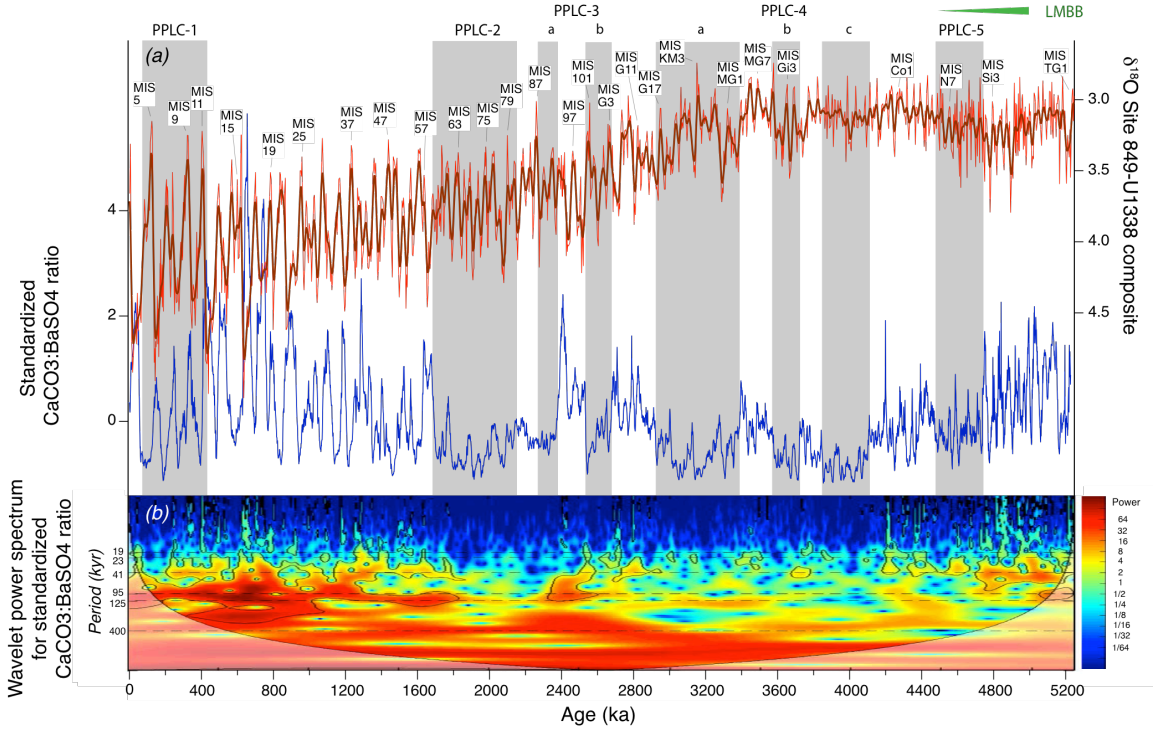

Figure 8: (a) A comparison of the stacked $CaCO_3$:$BaSO_4$ record of dissolution cycles to the combined U1338-849 isotope record. A strong 100-kyr periodicity to the dissolution cycle begins roughly at MIS 58, with low dissolution associated with periods of high benthic $\delta^{18}O$ (high ice volume). Before MIS 57, the association is less clear. (b) Wavelet analysis of the CaCO3:BaSO4 stack, showing 400 kyr power throughout the $CaCO_3$:$BaSO_4$ record and development of 100 kyr power in the interval between 2000 and 1500 ka that continues to the Recent.

Clim. Past Discuss., https://doi.org/10.5194/cp-2018-157
Manuscript under review for journal Clim. Past
Discussion started: 7 December 2018

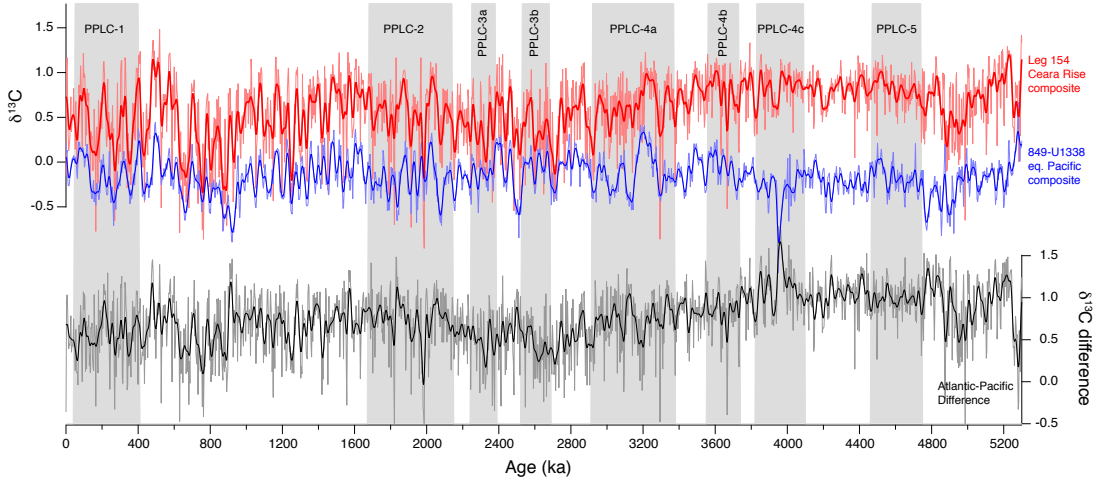

Figure 9: $\delta^{13}C$ records from Ceara Rise (Atlantic, red) and the Site 849-U1338 composite (Pacific, blue), and the Atlantic-Pacific $\delta^{13}C$ difference (black). The PPLC-4 dissolution interval falls on the period of decline of the Atlantic Pacific difference caused by a decrease in Atlantic $\delta^{13}C$ of about 0.7‰ between 4000 ka and 2500 ka, and an increase in Pacific $\delta^{13}C$ of about 0.4‰ over the same interval.

Clim. Past Discuss., https://doi.org/10.5194/cp-2018-157
Manuscript under review for journal Clim. Past
Discussion started: 7 December 2018

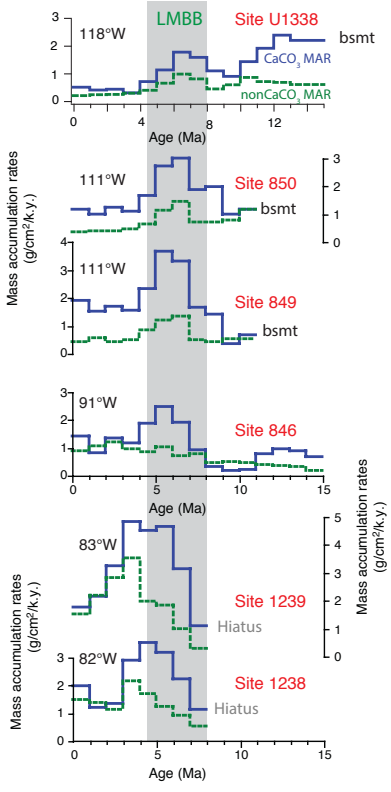

Figure 10: 1 Myr increments of $CaCO_3$ MAR (blue lines) and non-$CaCO_3$ MAR (Green dashed lines) on a longitudinal equatorial transect from 118°W to 82°W, near South America. Basement is marked by "bsmt". Data for U1338 is from this paper, while the other data are from ODP Leg 202 Shipboard Scientific Party (2003). The 8-4.5 Ma LMBB window is shaded. The end of peak $CaCO_3$ deposition is roughly 2 million years younger near South America than in the west. Non-$CaCO_3$ deposition is mostly biogenic silica at these drillsites. Eastern Pacific drill sites (Sites 846, 1238, and 1239) have increased biogenic deposition post-LMBB, presumably because of nutrient concentration after the Central American Seaway closed.